

Article

Techno-Economic Optimisation for a Wave Energy Converter via Genetic Algorithm

Sergej Antonello Sirigu *, Ludovico Foglietta, Giuseppe Giorgi, Mauro Bonfanti,
Giulia Cervelli, Giovanni Bracco and Giuliana Mattiazzo

Department of Mechanical and Aerospace Engineering, Politecnico di Torino, 10129 Turin, Italy; ludovico.foglietta@studenti.polito.it (L.F.); giuseppe.giorgi@polito.it (G.G.); mauro.bonfanti@polito.it (M.B.); giulia.cervelli@polito.it (G.C.); giovanni.bracco@polito.it (G.B.); giuliana.mattiazzo@polito.it (G.M.)

* Correspondence: sergej.sirigu@polito.it

Received: 9 June 2020; Accepted: 24 June 2020; Published: 30 June 2020



Abstract: Although sea and ocean waves have been widely acknowledged to have the potential of providing sustainable and renewable energy, the emergence of a self-sufficient and mature industry is still lacking. An essential condition for reaching economic viability is to minimise the cost of electricity, as opposed to simply maximising the converted energy at the early design stages. One of the tools empowering developers to follow such a virtuous design pathway is the techno-economic optimisation. The purpose of this paper is to perform a holistic optimisation of the PeWEC (pendulum wave energy converter), which is a pitching platform converting energy from the oscillation of a pendulum contained in a sealed hull. Optimised parameters comprise shape; dimensions; mass properties and ballast; power take-off control torque and constraints; number and characteristics of the pendulum; and other subcomponents. Cost functions are included and the objective function is the ratio between the delivered power and the capital expenditure. Due to its ability to effectively deal with a large multi-dimensional design space, a genetic algorithm is implemented, with a specific modification to handle unfeasible design candidate and improve convergence. Results show that the device minimising the cost of energy and the one maximising the capture width ratio are substantially different, so the economically-oriented metric should be preferred.

Keywords: wave energy; wave energy converter; PeWEC; techno-economic optimisation; genetic algorithm; cost of energy; CaPex; CWR

1. Introduction

Based on the gradual depletion of conventional fossil fuels, and most importantly, the established awareness of their destructive impact on the environment, recent years have witnessed a compelling momentum towards the energy transition and decarbonisation, shared by industry, governmental bodies and policy-makers. A condition for effective and reliable energy procurement is diversification, especially concerning renewable sources, which are usually more variable and volatile. Ocean energy, wave energy in particular, can play a major role in the overall energy mix, thanks to its high power density and availability [1]. Despite its potential, wave energy still remains substantially untapped since several challenges, hindering commercialisation at industrial scale, remain to be overcome. Wave energy conversion is yet to reach economic viability and is not competitive with other renewable energy technologies, due to an excessive LCOE (levelised cost Of energy) at the current stage of development.

From a high-level perspective, one of the main reasons for the unsuccessful development of effective technologies is that typical development pathways prefer to rapidly increase readiness levels before an acceptable performance is achieved [2]. Considering a matrix composed of technology readiness level (TRL) and the technology performance level (TPL), deficient development pathways tend to

increase TRL first, at low TPL; conversely, optimal trajectories should increase TPL first, at low TRL, and then increase TRL towards commercialisation [3]. Although it is challenging to perform an accurate estimation of some performance aspects at low TRL, due to inherent limitations of small-scale devices and subsystems, techno-economic aspects should be taken into account. Changing such a development paradigm involves adopting better design practices, since common approaches are inherently suboptimal. In particular, often, design is performed in sequential fashion, considering different parts of the power conversion chain independently. A representative example is the optimisation of the hydrodynamics and power absorption of an uncontrolled device, followed by a design of an optimal controller, followed by the inclusion of technical constraints and efficiency, finally reaching the stage of cost evaluation and reduction. Although such an incremental approach is justified by the complexity of the system, neglecting mutual interaction typically leads to a suboptimal solution.

An effective design requires one to follow a holistic approach, based on representative wave-to-wire mathematical models [4], including some energy-maximising control strategy [5,6] considering technological constraints [7,8] and costs [9], since all of such aspects are tightly interrelated. Representative hydrodynamic models are advisable, since a controlled device may be affected by strong nonlinearities with major negative effects on power production [10]. Furthermore, unconstrained linear or partially-linear models may predict unrealistic behaviour under the action of an optimal controller [11], which is also sensitive to modelling errors [12,13]. Note that it is essential to include an energy-maximising control strategy, since it has the ability to significantly increase power-production performance over the operational sea states. Moreover, the control strategy has a great influence on the dynamic characteristic of the response of the device [14], making the power-wise optimal solutions for uncontrolled and controlled conditions significantly different [15]. However, the ability of the controller to optimise power absorption is highly dependent on physical constraints, mainly on displacement, speed and force/torque [16]. Such constraints depend on the electrical and mechanical subcomponents characteristics, and ultimately, cost. On the other hand, the hydrodynamic behaviour of the device mainly depends on its shape and dimensions, which entail volume and mass, which are main drivers of capital cost.

A practical implementation of an all-encompassing design optimisation is challenging, mainly due to the vast multi-dimensional search space which cannot be tackled with conventional global optimisation approaches due to computational limitations. Moreover, often there is no analytical representation of the relationship between input and output variables, due to hydrodynamic curves defined by points through panel-based simulations (BEM) and implicit nonlinearities requiring simulation via time-advancing schemes [17], or in some conditions, harmonic balance [18]. Therefore, both cost function and constraints usually behave as grey or black boxes. For such problems, genetic algorithms are among the most common choice, since they can handle design spaces of high dimensionality and complex cost functions and constraints, without relying on the knowledge of their mathematical structure [19]. Genetic algorithms are metaheuristic optimisation codes based on the evolutionary theory, relying on the survival-of-the-fittest principle. Thanks to their stochastic approach, they favour the identification of the global optimum, reducing the risk of convergence to a local minimum. Furthermore, they impose no specific requirement on the system to be optimised, since it is treated as a black box. Genetic algorithms are used in this paper based on previous experience of the authors, although other metaheuristic approaches exist, able to handle a large parameter space, such as covariance matrix adaptation, differential evolution and particle swarm algorithms [20].

Following their use in the general marine engineering field [21], genetic algorithms recently gained popularity in the wave energy field, but are mainly used for the optimisation of the array layout of several wave energy converters (WECs) [22,23]. Although scarce, some single WEC design optimisations via genetic algorithm are found in the literature. Reference [24] optimised the radius and draft of an archetypal cylinder, maximising the absorbed power and bandwidth. The design space is bi-dimensional; the geometry is idealised; and the power take-off (PTO) is a simple linear damper with a frequency-independent damping coefficient. Since power is not an effective single-objective function for practical design, Ref. [25] introduces proxies for costs, structural loads and PTO rating

loads into the objective function. Costs are assumed to be proportional to the submerged surface and the maximum reaction force. While [25] considered fixed-axis devices of conventional shape, Ref. [26] attempted to generalise the geometry as much as possible, using B-splines to describe wetted surfaces of arbitrary shapes. Moreover, frequency-dependent energy-maximising control is introduced, also including constraints to limit unrealistically large amplitudes of motion that follow. As a proxy for costs, length and displaced volumes are considered in the cost functions. Finally, Ref. [27] proposes a thorough optimisation of the SEAREV device, attempting to maximise the produced power while minimising the device mass (as a crude proxy for costs), including various constraints and latching-declutching control.

This paper proposes a comprehensive techno-economic optimisation of the PeWEC (pendulum wave energy converter), which is a self-reacting WEC extracting energy from the oscillation of a pendulum sealed in a floating hull [28]. Several novelties, with respect to other design optimisation of WECs, are included. First and foremost, similar only to [27], a high level of detail of a realistic device is considered, as opposed to archetypal or generic geometries. However, a wide design space with high dimensionality is investigated, counting up to 13 design variables, comprising shape and dimensions of the floater; ballast and inertial properties; pendulum properties and numerosity; PTO rated torque; velocity and power; and gearbox speed conversion ratio. Moreover, realistic geometrical, technical and structural constraints are implemented, based on subcomponents characteristics. No idealised proxy is used for estimating costs, which are directly computed based on the cost of different material used for construction and different PTOs from a catalogue. Finally, a simple but realistic energy-maximising control strategy is implemented, including explicit constraint handling, in order to perform a control-informed optimisation. Due to the high-dimensionality and mutual dependence of design variables, a stochastic optimisation approach, treating different variables as independent and random, encounters a high level of unfeasible combinations, which may potentially hinder the success of the optimisation. In order to deal with unfeasible solutions, a tournament-based genetic algorithm is implemented, reducing the impact of mortality rate on the convergence rate. The objective function, which the genetic algorithm tries to minimise, is the ratio between capital cost and annual energy production (AEP). However, in order to highlight the impact of the performance index and to generate a Pareto front, the capture width ratio is also considered as an additional objective. It is shown that hydrodynamic efficiency and cost of energy are contrasting objectives; therefore, this paper provides evidence that challenges the common practice of optimising the hydrodynamic performance during early-stage development, suggesting companies should pursue economic performance instead.

The remainder of the paper is organised as follows: Section 2 describes the technology while Section 3 presents its parametrisation for the optimisation algorithm, also focusing on constraints, cost functions and different objective functions. Finally, Section 4 provides main significant results with a critical discussion. Some final remarks are given in Section 5. Appendix A provides full general details about the genetic algorithm that effectively deals with discrete multi-variate problems with high mortality rate.

2. Technology

The system under consideration in this optimisation study is the PeWEC, an acronym of pendulum wave energy converter. PeWEC is a self-referenced inertial-based floating WEC, composed of a sealed hull enclosing a pendulum and the power take-off (PTO). There are notional similarities between PeWEC and the SEAREV device [29], both based on an inertial-activated body contained in a floating hull; however, while SEAREV is designed for ocean applications, PeWEC is initially aiming at lower energetic closed seas with lower-period waves (e.g., the Mediterranean Sea). The device is anchored to the seabed by means of a 3-line-3-segment mooring system, with each line composed of a jumper (riser) and a clump-weight [30]. When the device is moved by the waves, a relative motion between the hull and the internal pendulum is obtained, mostly due to the pitching motion. The kinetic energy related to this movement is converted into electrical energy by the PTO connected to the pendulum's hinge. A control law is implemented in the PTO driver to adjust the pendulum dynamics to the instantaneous

sea conditions, with the purpose of maximising the output energy. A schematic of the PeWEC system is shown in Figure 1.

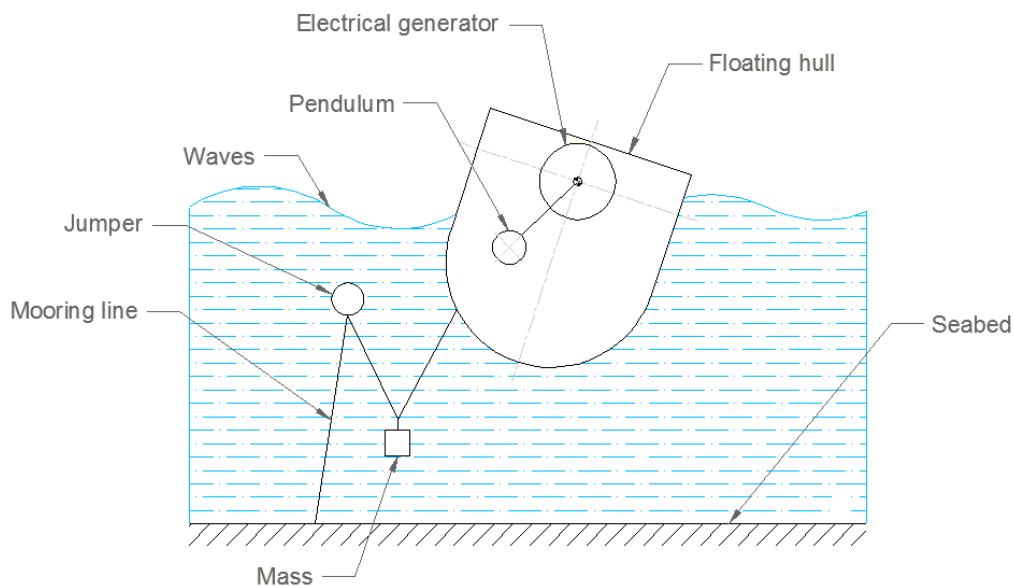


Figure 1. Schematic of the PeWEC working principle. Incoming waves excite the floating hull in pitch, transferring energy to the oscillation of an inner pendulum, whose motion is damped by a PTO. Three 3-segment mooring system, composed of a jumper and a clump-weight, keeps the system in place.

The hull is a sealed steel structure composed of a curved keel, two side walls and a flat topping; three internal sand ballasts (on the keel, stern and bow) ensure the mass distribution necessary to guarantee the required inertial properties, while a trellis structure is used to support the pendulum and the electronic equipment. The pendulum is composed of a cylindrical steel oscillating mass and a shaft, which is connected to the PTO system through a gearbox that ensures an appropriate coupling between the pendulum oscillation velocity and the PTO nominal speed. In order to extract energy from the pendulum movement, the PTO generates a reaction torque, which is adjusted by the driver's control system. Such constructive and technical features, based on early-development of the device, are here optimised via genetic algorithm. The technology has already been proven to be effective and promising, mainly thanks to wave tank tests at 1:45 and 1:12 scales [31]. Figure 2 shows a 3D digital model of the 1:45 prototype while Figure 3 shows a photo of the 1:12 prototype in the testing wave tank.

The concept of PeWEC germinated from the ISWEC (inertial sea wave energy converter), which generates the inertial coupling between PTO and the hull by means of the gyroscopic effect of a spinning flywheel [32]. While ISWEC requires power to keep the flywheel in rotation and create the self-reaction force [33], PeWEC is entirely passive, hence reducing explicit power loss sources. Further technological improvements are being explored for both the PeWEC and the ISWEC in order to increase the overall power conversion efficiency, such as resonant U-tanks [34], advanced control techniques [35], estimation and forecasting [36]. Moreover, the mooring system is under development, since it can affect the device performance [37]. However, this paper deals with a more fundamental early holistic optimisation of the PeWEC device shape, geometry and subcomponents, as further discussed in Section 3. The mathematical model, used to predict motion and loads of a given device, is presented in Section 2.1. The strategy to parametrically define multiple devices that the genetic algorithm can automatically optimise is presented in Section 3.

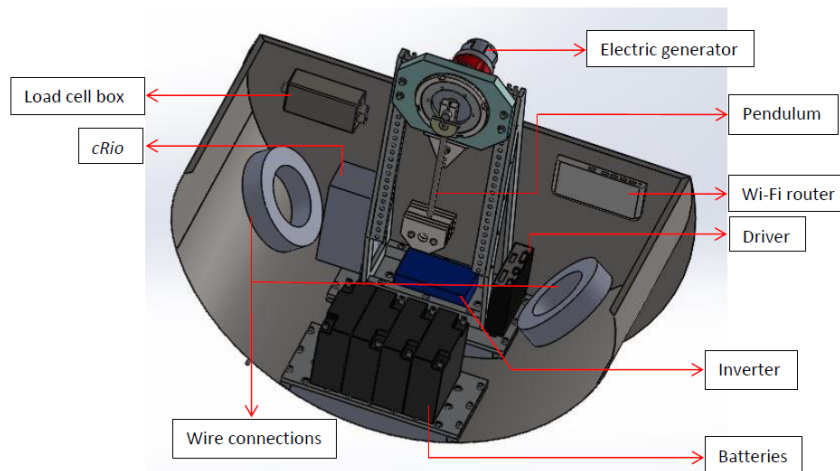


Figure 2. Digital representation of the 1:45 PeWEC prototype and its subcomponents.

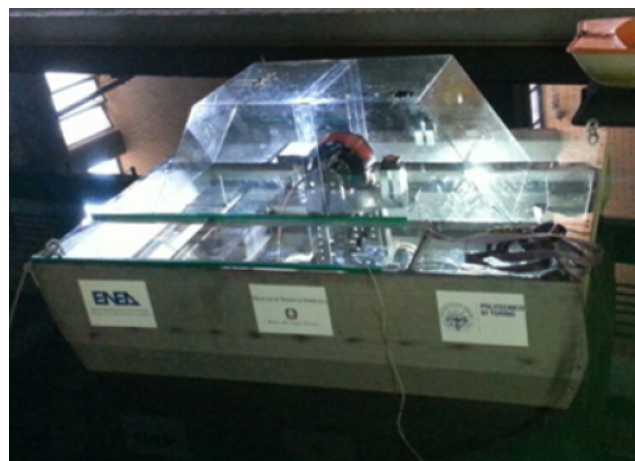


Figure 3. Photo of the 1:12 PeWEC prototype tested a wave tank [31].

2.1. Mathematical Model

The optimisation software relies on a mathematical model to evaluate the objective function which, in this paper, depends on the response of the device to incoming waves. An essential requirement for such a mathematical model is low computational speed, since a high number of individuals (order of tens of thousands) have to be assessed in a reasonable time. Therefore, a fully-linear model based on linear potential flow is implemented in frequency domain, thanks to its computational convenience. However, in order to avoid unrealistic motion that a linear model would predict under controlled conditions, various constraints are included, as further discussed in Section 3.2. Potential-flow-based models are conceptually divided into two phases: Firstly, the linear hydrodynamic curves, namely, excitation coefficients (F_w), added mass (**A**) and radiation damping (**B**), are evaluated at a representative set of frequencies by means of a boundary element method (BEM) software, such as NEMOH [38] (this must be automatised in the genetic algorithm). Secondly, the dynamic response of the device is evaluated for a comprehensive set of sea states, characteristic of the designed installation site, taking care of determining appropriate energy-maximising control parameters. Although the run time of BEM codes depends on the number of simulated frequencies and on the discretised geometry, it is of the order of magnitude of 10^2 s, on average. Since shape and dimensions of the hull are among the optimisation parameters, a detailed description is provided in Section 3.1. On the other hand, the structure of the dynamic response simulator is invariant:

$$[\mathbf{M} + \mathbf{A}(\omega)] \ddot{\mathbf{X}} + \mathbf{B}(\omega) \dot{\mathbf{X}} + (\mathbf{K}_h + \mathbf{K}_p) \mathbf{X} = A_w(\omega) \mathbf{F}_w(\omega) + \mathbf{T}_{PTO} \tag{1}$$

where \mathbf{M} is the mass matrix, \mathbf{K}_h is the hydrostatic stiffness, \mathbf{K}_p the restoring force of the pendulum, A_w is the wave amplitude, \mathbf{T}_{PTO} is the PTO action and \mathbf{X} is the state vector. Under the assumption of mono-directional waves aligned with the longitudinal axis of the hull, a planar motion of the hull can be assumed, namely, in surge (x), heave (z) and pitch (δ). Including the pendulum oscillation (ε), the state vector has four dimensions:

$$\mathbf{X} = \begin{bmatrix} x \\ z \\ \delta \\ \varepsilon \end{bmatrix} \tag{2}$$

The PTO acts on the rotational degree of freedom of the pendulum, applying active and reactive power, proportional to displacement and velocity with constant coefficients, k_{PTO} and c_{PTO} , respectively:

$$\mathbf{T}_{PTO} = \begin{bmatrix} 0 \\ 0 \\ 0 \\ -k_{PTO}\varepsilon - c_{PTO}\dot{\varepsilon} \end{bmatrix} \tag{3}$$

Coupling between the pendulum and the hull is provided by the restoring force of the pendulum and inertial reaction forces, which are expressed in \mathbf{K}_p and \mathbf{M} , respectively. After linearisation [39]:

$$\mathbf{K}_p = \begin{bmatrix} 0 & 0 & 0 & 0 \\ 0 & 0 & 0 & 0 \\ 0 & 0 & -gm_p(d-l) & gm_p l \\ 0 & 0 & gm_p l & gm_p l \end{bmatrix} \tag{4}$$

$$\mathbf{M} = \begin{bmatrix} (M + m_p + m_b) & 0 & m_p(d-l) & -m_p l \\ 0 & (M + m_p + m_b) & 0 & 0 \\ m_p(d-l) & 0 & I_y + I_p + I_b + m_p(d-l)^2 & I_p + m_p l^2 - m_p d l \\ -m_p l & 0 & I_p + m_p l^2 - m_p d l & I_p + m_p l^2 \end{bmatrix} \tag{5}$$

where M is the mass of the hull; I_y is the hull moment of inertia; g is the acceleration of gravity; d is the distance between the device centre of gravity (CoG) and the pendulum fulcrum; l is the pendulum length; m_p and m_b are the masses of the pendulum and the bar holding the pendulum, respectively, and I_p and I_b are their moments of inertia, respectively.

In order to maintain the model linear, mooring effects are neglected, as are mean drift forces and second order effects. Moreover, viscous effects are neglected, since they would require specific tuning for each device [40]. However, the linearised model has been validated through an experimental campaign [39], ensuring appropriate accuracy and representativeness for global design optimisation problems [41]. Nevertheless, it is worth noticing that these assumptions (planar waves and motion, and absence of a mooring system) are simplifications, since real waves may be short-crested, inducing complex motion in 6 degrees of freedom, which is also possible due to parametric instabilities and nonlinear coupling [42], and the mooring system may significantly affect the dynamics of the system [37].

The fully-linear model can be efficiently solved in the frequency domain with a very low computational time. For each wave, the optimal k_{PTO} and c_{PTO} are sought by means of a multi-variate simplex algorithm [43], respecting global constraints on loads and displacements, as discussed in Section 3.2.

It is worth remarking that the optimal control (performed by the simplex algorithm for each device) is completely independent of the design optimisation (performed by the genetic algorithm modifying geometrical and technical characteristics of the device). For each individual, the response to each irregular wave (modelled according to a Jonswap spectrum), comprising the simplex optimisation, requires about one second of computation. The productivity is computed over a scatter diagram densely described by 128 waves, accounting for about 100–150 seconds of computation. The targeted installation site is near Pantelleria island, in the Mediterranean Sea. The set of representative waves is chosen in order to adequately cover areas of the scatter diagram with non-negligible occurrence, as shown in Figure 4.

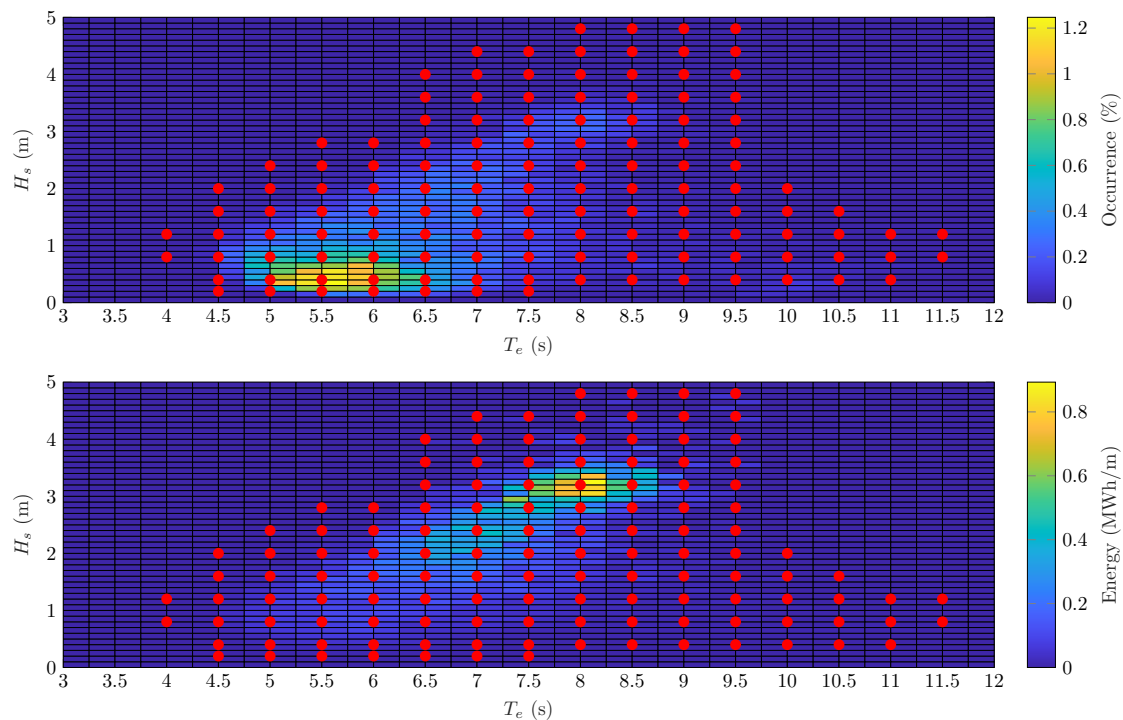


Figure 4. Occurrences and energy scatter diagrams for the installation site close to Pantelleria island, Italy; 128 representative waves were selected for the productivity estimation, shown by the red markers, where the occurrence percentage is not negligible.

3. Optimisation Software

The implementation of the optimisation software, as presented in Figure A1 and discussed in Appendix A, requires the definition of the design variables, the objective function and the tuning parameters of the genetic algorithm. The system, presented in Section 2, has virtually an infinite number of design variables that define its hydrodynamic behaviour, inertial properties and power absorption/conversion characteristics. Therefore, making some assumptions on the geometry and subcomponents is mandatory. Moreover, a parametric definition is required, allowing the software to fully define the system without direct human intervention. Section 3.1 details such a parametric representation, univocally identifying a device by its shape, dimensions, mass, inertia, ballast’s distribution, pendulum and PTO characteristics. Starting from the shape of the hull, a BEM code automatically computes hydrodynamic curves, used to predict the device response to waves. However, techno-economic considerations should be included in the optimisation process, as extensively discussed in Section 1. Section 3.2 provides all functions that are used to estimate the cost of material and components. Moreover, constraints are imposed on displacements, velocities and loads, in accordance to the characteristics (and costs) of subcomponents. Finally, Section 3.3 presents tuning parameters of the genetic algorithm and the definitions of different performance indexes that the software aims at optimising.

3.1. Parametric Definition

In this work, 13 parameters are chosen to describe the device, summarised in Table 1 and hereafter discussed in detail: six for the hull, five for the pendulum and two for the PTO.

The shape of the hull is based on previous experience matured during the development of the PeWEC devices. For both manufacturability and hydrodynamic performance, the hull profile is assumed to be composed of a bottom circumference, tangential to two circumferences in the bow/stern sections, as shown in Figure 5, while the transversal section is assumed to be constant. The floater is symmetric with respect to the y - z and x - z planes and it results from the extrusion of the floater profile shape along the y -axis. The x -axis coincides with the floater deck and the z -axis goes from the deck of the floater upwards. The smooth surface with large radius of curvature is easier and cheaper to manufacture [44]. Moreover, the absence of sharp edges in the hull profile guarantee a low impact of vortex shedding and viscous drag losses [41]. Finally, the absence of re-entrant angles significantly reduces the risk of slamming events [27].

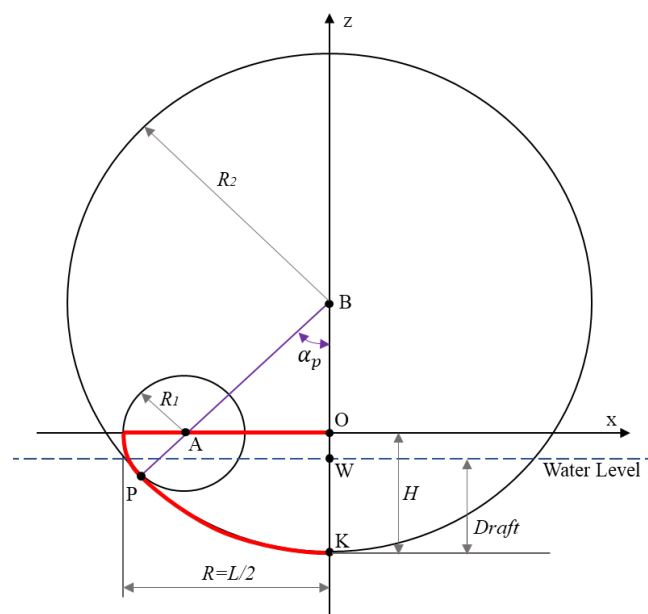


Figure 5. Parametric definition of the cross section of the floater.

The following relevant parameters, with respect to Figure 5, characterise the hull’s profile:

- R : semi-length of the floater;
- H : overall height of the hull—i.e., the distance between the keel and the deck;
- D : draft of the hull;
- R_1 : radius of circumference C_1 ;
- (x_A, z_A) : x - and z -coordinates of the centre of C_1 , respectively, with $z_A = 0$;
- R_2 : radius of circumference C_2 ;
- (x_B, z_B) : x - and z -coordinates of the centre of C_2 , respectively, with $x_B = 0$;
- $\alpha_p = \angle PBO$.

A subset of six independent geometrical and inertial parameters is defined, which are used as design parameters in the genetic algorithm:

- L : length of the floater;
- W : width of the floater;
- $h = x_A/R$: bow/stern circumference ratio;

- $k = H/R$: height ratio;
- $j = D/H$: draft ratio;
- BFR: ballast filling ratio, defined as the ratio of ballast located in aft/fore ballast tanks over the total ballast (BFR = 1: all the ballast is stored in aft/fore ballast tanks; BFR = 0: all the ballast is stored in bottom ballast tank).

Figure 6 shows four examples of the effects of the geometric parameters h and k . Figure 7 shows examples of draft and ballast allocation; namely, j and BFR. Note that the amount of ballast required (M_{bal}) is univocally defined by the mass of the displaced volume of water (M_{tot}), the mass of the hull structure (M_h) and the mass of the pendulum-PTO units. The allocation of M_{bal} between bow/stern and keel compartments determines the total moment of inertia of the system, which is an important parameter to conveniently change the resonant period in pitch. The ballast material is assumed to be sand, with density (ρ_{bal}) of 1400 kg m^{-3} , which is considered to be an appropriate compromise between cost and specific weight. Filling of the ballast compartments is assumed from the extremities inwards, providing higher inertia and being easier from a practical point of view.

The hull is made out of standard naval carpentry steel, with a density (ρ_h) of 7800 kg m^{-3} . Based on previous experience with prototyping of the PeWEC device, M_h is assumed to be 90 times the total volume of the floater. Consequently, assuming the walls of the floater as thin plates, an equivalent thickness is computed from the lateral surface of the floater and M_h , making the computation of inertial properties of the hull possible.

On the hull's centreline, multiple pendulums can be placed, and their number (N_p) is one of the design parameters of the genetic algorithm. Each pendulum is composed of an oscillating cylindrical steel-made mass and a steel shaft. A trellis structure envelopes and supports the pendulum, a gearbox and the PTO; the ensemble of these components is referred to as unit, and its mass, inertia and volume are parametrically estimated starting from the pendulum's properties. The mass and inertia of the entire unit are 20% and 30% higher than the mass and inertia of the pendulum, respectively. The extension of the unit in the y -direction is 2 m longer than the pendulum dimension, in order to account for the required space for machinery and technical operators during assembly and maintenance. The overall mass of the device depends on the submerged volume, defined by j , k and L . Since the mass of the hull is proportional to its total volume, the remaining part has to be composed of the ballast and units. A design parameter (β_U) is defined so that the mass of each unit is:

$$M_{unit} = \frac{\beta_U (M_{tot} - M_h)}{N_p} \quad (6)$$

Consequently, the ballast mass is the complementary fraction of β_U .

Each pendulum is composed of a cylinder with axis parallel to the y -direction, swinging around a fulcrum. The volume of the cylinder is computed from its mass and density ($\rho_p = 7800 \text{ kg m}^{-3}$). Known volume, radius and height are defined by a shape factor (σ_p), which is a free design parameter deciding if the pendulum is large and short ($\sigma_p = 0$) or small and long ($\sigma_p = 10$), with respect to the available space. Once the geometry is defined, the length of the swinging arm of the pendulum is defined by a design ratio γ_p , which takes the available space in the hull into account. Finally, the height of the fulcrum is defined by a further design parameter λ_p . Note that the relative geometry of the hull and the pendulum allow for full rotation of the swinging mass around the fulcrum.

Note that not all possible combinations of geometric and pendulum property parameters are feasible due to volume and weight physical restrictions. Consequently, during the optimisation, unfeasible individuals are discarded and the death penalty function is computed, contributing to increase the mortality rate of the genetic algorithm.

Finally, the actual conversion stage is performed by a permanent magnet synchronous motor (PMSM), one for each pendulum, combined with a planetary gearbox that is well suited for high torque and low speed applications. The gearbox ratio r_g is a further design parameter. Finally, different PTO systems are

used (ID_{PTO}), with different combinations of nominal speed (n_{PTO}) and nominal torques (T_{PTO}), hence the costs, as shown in Figure 8.

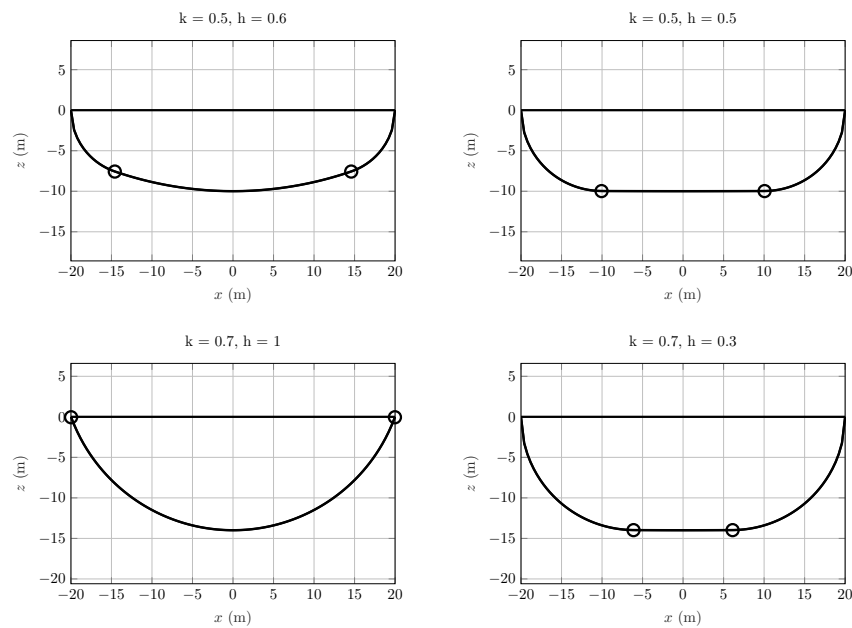


Figure 6. Examples of the effects of the h and k geometric design parameters.

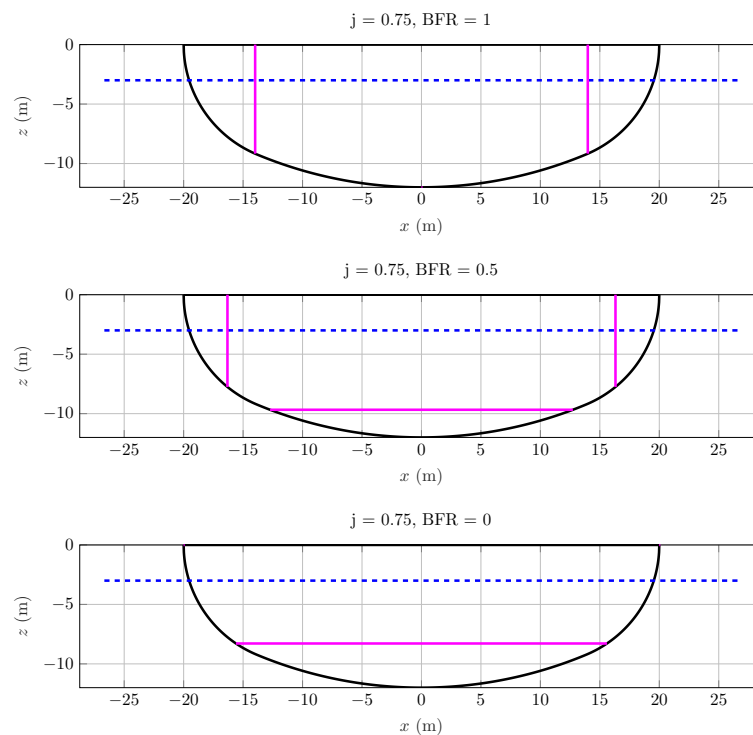


Figure 7. Examples of the effects of the j and ballast filling ratio (BFR) design parameters.

A summarising table of the 13 design parameters is provided in Table 1, including lower and upper bounds, and number of equally spaced steps. Bounds and step sizes are based on the authors' experience in developing the technology and running the model, ensuring that the minimum allowed variations of the design parameters produce small but relevant variations in the device performance. In this way, the algorithm is forced to consider only substantially different individuals, preventing the risk of simulating almost-equal devices. Although this objective could be achieved with a continuous

parameter space by applying appropriate tolerances and checks on parameter variations, the authors believe that a gridded approach is more convenient, since it is easier to inspect and implement.

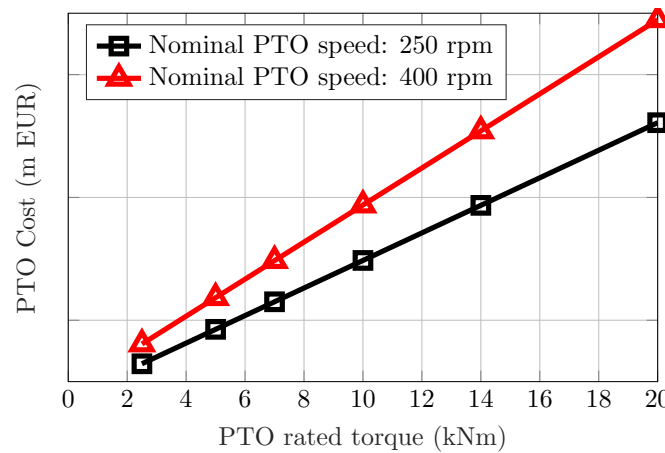


Figure 8. Cost of each power take-off, linearly proportional to the rated torque, with slope depending on the nominal speed.

Table 1. Thirteen design parameters used by the genetic algorithm to univocally define an individual, as discussed in Section 3.1. Discrete values with constant spacing are used, with lower and upper bounds.

Design Parameter	Symbol	Units	Lower Bound	Upper Bound	# Discretisation
Hull length	L	(m)	8	30	23
Hull width	W	(m)	5	30	26
Bow/stern circumference ratio	h	(-)	0.5	1	6
Height ratio	k	(-)	0.5	1	6
Draft ratio	j	(-)	0.65	0.8	4
Ballast filling ratio	BFR	(-)	0.5	1	6
Number of pendulum/PTO	N_p	(-)	1	15	15
Unit mass ratio	β_U	(-)	0.05	0.95	18
Pendulum shape factor	σ_p	(-)	0.05	0.95	10
Pendulum arm factor	γ_p	(-)	0.1	1	10
Pendulum fulcrum factor	λ_p	(-)	0.1	1	10
Gearbox ratio	r_g	(-)	10	30	3
PTO ID	ID _{PTO}	(-)	1	11	11

3.2. Techno-Economic Definitions and Constraints

The definition of the fitness index beholds primary importance in the identification of an optimal device: the genetic algorithm, similarly to other optimisation codes, iteratively tests several devices to find the one that minimises the objective function. In this work, three different fitness functions are used in three independent optimisation cycles, in order to have a deeper understanding of the phenomenon by building the Pareto front. In fact, multi-objective algorithms are usually performed as several single-objective optimisations where the performance index is computed as a weighted average of the multiple objectives [45].

The first objective is to minimise the capital expenditure (CapEx) over productivity (CoP) ratio, computed as the ratio between the overall capital expenditure (CapEx) and the produced energy over the lifetime of the plant (N_y , assumed 25 years for PeWEC):

$$\text{CoP} = \frac{\text{CapEx}}{N_y \text{ AEP}} \tag{7}$$

where the annual energy production (AEP) is computed considering net power, affected by efficiencies and baseload: the gearbox is assumed to have a 0.95 mechanical efficiency; the PTO conversion system is considered to have a conversion efficiency of 0.95; the baseload considers all the electrical machinery input energy necessary for their correct operation: 500 W for each pendulum. Power losses from the bearings have been neglected, since the pendulum rotates at low speed [39].

The overall cost considers the device’s capital expenditures to be classified in three main terms: hull’s materials and construction, units’ materials and construction, PTO. The mooring system is not considered, since its layout and cost are device-specific and no clear automatic parametrisation could be tackled in such an early design stage. Similarly, operational and maintenance expenditure (OpEx) is not considered in this work: on the one hand, its assessment requires extensive experience and a mature technology; on the other hand, in sealed WECs such as PeWEC but also ISWEC and SEAREV, OpEx is usually negligible compared to CapEx, since there are no moving parts subject to hostile marine environment (salty water, dust and debris). In fact, for common WECs presenting moving parts in hostile environment, it is estimated that the CapEx accounts for up to 35% only [46]. However, for the SEAREV device (with all moving parts enclosed in a sealed hull, as the PeWEC) it is estimated that OpEx is about 2% of the overall expenses [27]. Moreover, in such conditions, the levelised cost of energy (LCOE) is shown to be mainly sensitive to AEP and CapEx, while OpEx, inflation rate, lifetime and expected internal rate of return are less impactful [27].

Several PTO models are considered in this analysis; each of them is characterised by its own maximum and nominal values in torque and speed. PTO costs are assumed to be significantly proportional to the nominal torque, with slope proportional to the nominal velocity, as shown in Figure 8. The PTO costs comprise those of the generator, the gearbox and various power electronic ancillary systems. However, the explicit costs of PTOs have been hidden for confidentiality. Note that a larger PTO provides higher freedom to the controller and is able to convert more energy. However, such a flexibility requires higher investments. The optimisation algorithm attempts to find a suitable compromise, also taking into account technical constraints on speed, torque and power of the PTO.

Material and manufacturing costs of the hull (C_h) and the pendulums (C_p) are estimated to be proportional to their respective mass, with the specific cost of the pendulums being almost twice the specific cost of the hull. Although simplified, all cost functions (PTO, hull construction and pendulum construction) are notionally based on the experience of the authors in the development and deployment of actual small and full-scale devices.

As discussed in Section 1, it is advisable to optimise the overall CoP, since it takes into account the compromise between techno-economic performance and hydrodynamic performance. However, a popular approach in the literature is to optimise the AEP or the hydrodynamic absorption abilities, regardless of the cost and/or technical characteristics and the limitations of the subcomponents required to achieve such a high conversion efficiency. In order to highlight substantial differences in convergence direction and the obtained optimal device, a second objective is considered: the capture width ratio (CWR), which is a common measure of energy conversion ability, defined as ratio between AEP and annual energy available in the resource (E_w):

$$CWR = \frac{AEP}{E_w} \tag{8}$$

Note that the correspondent performance index (to be minimised) is defined as -CWR, since CWR should be maximised. For each sea state, the incoming wave power on the device is defined as:

$$P_w = \frac{\rho g^2}{64\pi} H_s^2 T_e W \tag{9}$$

where ρ is the water density, H_s the significant wave height and T_e the energy period. Equation (9) shows how the incoming available energy is proportional to the width, which is one of the main design parameters in the optimisation. In practice, while maximising AEP will likely maximise (W) in order

to have access to larger power, maximising CWR seeks to increase the portion of the converted energy from the wave to the grid, regardless of price of conversion. Finally, maximising CoP focuses on the cost of the conversion, regardless of its efficiency.

Since there are two competing objectives (minimising CoP and maximising CWR), a multi-objective optimisation approach is adopted. By means of a scalarisation technique [47], the two different objectives are aggregated into a unique objective by means of a weighted average, using a pair of weights (w_1, w_2). Through the choice of different weights, it is possible to build the Pareto-optimal set. Three pairs of weights have been considered, as shown in Table 2. Effectively, sets (1) and (3) are single-objective optimisations, while set (2) is a proper multi-objective one. However, by aggregating the results of the three optimisations, a Pareto front can be constructed.

Table 2. Multi-objective weights.

Weight Set ID	Explanation	CoP-Weight (w_1)	CWR-Weight (w_2)
(1)	CoP-driven	1	0
(2)	Weight-driven	0.5	0.5
(3)	CWR-driven	0	1

Technological constraints are applied to all three optimisations. For each sea state, the optimal control parameters are chosen in order fulfil constraints tabulated in Table 3. Note that velocity and torque constraints depend on the particular PTO and the gearbox installed, and hence on the design parameters ID_{PTO} and r_g , respectively.

Table 3. Technological constraints, fulfilled by tuning the control parameters.

Constrained Variable	Units	Constrained Value
$rms(\delta)$	(°)	15
$rms(\epsilon)$	(°)	40
$\max(\dot{\epsilon})$	(rpm)	n_{PTO}^{max}/r_g
$\max(T_{PTO})$	(kNm)	$T_{PTO}^{max}r_g$

3.3. Genetic Algorithm

In Appendix A, a detailed description of the genetic algorithm is provided. Considering the specific problem, presented in Section 3.1, the tuning factors of the algorithm in Table 4 were chosen. The MATLAB built-in implementation of the genetic algorithm has been used, along with its default tuning parameters, which are considered to be suitable. Although beyond of the scope of this paper, a throughout sensitivity analysis can potentially improve the convergence rate of the algorithm.

Table 4. Tuning parameters of the genetic algorithm, described in Appendixes A.1–A.6 and shown in red in the flow chart in Figure A1.

Name	Symbol	Value
Population size	N	150
Maximum generation count	M	200
Maximum stall generation	M_{Δ}	50
Convergence threshold	Δ	1.00×10^{-6}
Elitism percentage	ϵ	5%
Tournament size	k	4

4. Results

The MI-LXPM genetic algorithm has been chosen since it can effectively handle integer optimisation problems with potentially high number of unfeasible solutions. Figure 9 shows the development of the mortality rate through generations for the example of the CoP-driven optimisation. The first population has a significant number of unfeasible solutions, since it results from a purely stochastic process. However, the mortality rapidly drops to an average value (excluding the first two generations) of 25.5% with a standard deviation of 4.3%. Furthermore, note that there are 118 generations, meaning that the algorithm met convergence criteria before the maximum generation count of 200.

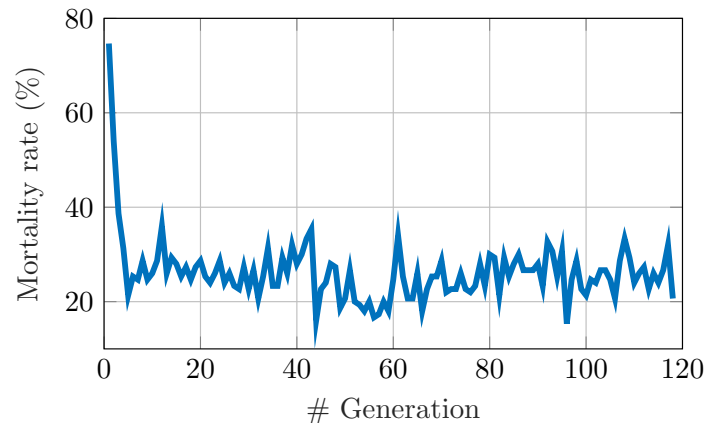


Figure 9. Mortality rate for the capital expenditure (CapEx) over productivity (CoP)-driven optimisation. Excluding the first two generations, the average is 25.5% and the standard deviation is 4.3%.

Note that two different seeds for the randomisation of the initial population of each optimisation have been used, reaching consistent results, hereafter discussed. The overall development of the algorithm is shown in Figure 10 for the example of the CoP-driven optimisation. The generic objective function f^* to be minimised is on the vertical axis. For each generation, individuals are sorted according to f^* , so that the N th individual has the highest f^* . Unfeasible individuals are missing markers at lowest individual count. The colour code is in accordance with the generation count, showing the evolution of the population. The final population count is 118, as also shown in Figure 9. Therefore, since the maximum stall generation criterion is 50 (see Table 4), improvements of the overall-optimum are found until generation 68. The cloud of points is also projected onto the vertical planes, highlighting relevant trends. The projection on the vertical right plane has the purpose of showing the potentially significant change of the slope as generations advance; i.e., if the ratio of fit individuals over the whole population changes. The fact that such a projection preserves about the same shape shows that the overall distribution of fit individuals remains about constant, apart from early generations. This is also shown in the projection on the vertical left plane: the minimum of f^* decreases as generations progress, as expected and desired; however, the improvement is abrupt in early generations (until generation 40) and slows down afterwards (until generation 68). Furthermore, the number of devices at a low f^* is relatively scarce, with a rarefied gap between the fittest individuals and the rest of the population. This suggests that the degradation of performance is quite sensitive to the choice and combination of design parameters. Moreover, the presence of about 20% of unfeasible devices may have an impact on the uniform improvement of the whole population. An alternative, smoother definition of the performance index, a finer parameter grid and different cross-over/mutation strength may smooth the convergence and increase the convergence rate. Moreover, the definition of the design parameters may be appropriately revised in order to structurally reduce the likelihood of unfeasible individuals. However, although such an extensive sensitivity analysis is an interesting topic for future investigation, it is believed that the current setup provides appropriate convergence and satisfactory results to discuss techno-economic aspects of the PeWEC device optimisation.

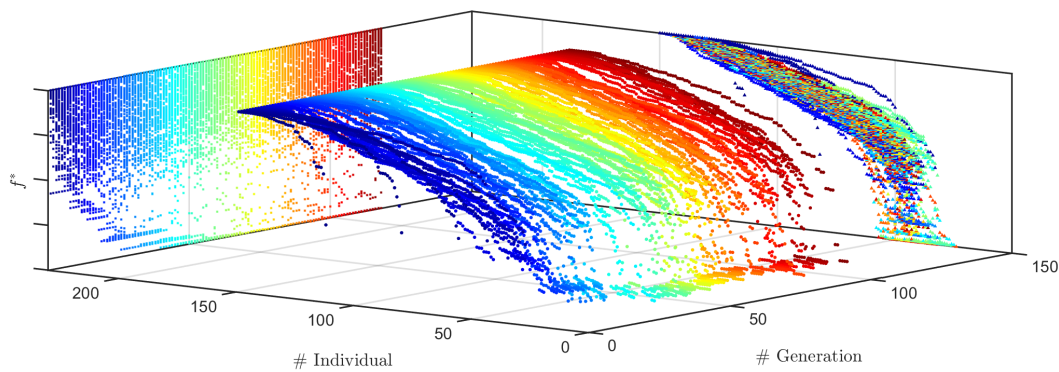


Figure 10. CoP-driven optimisation results: for each generation, individuals are sorted according to the objective function (f^*) to be minimised. The cloud of points is projected onto the vertical planes. The colour code corresponds to the generation count.

Three different optimisations have been performed, pursuing different objective functions in order to generate a Pareto front, as discussed in Section 3.2. Figure 11 shows the ensemble of all individuals generated from the three separate optimisations aggregated, plotting on the productivity versus the device cost, with the colour code being proportional to the CoP (left) and CWR (right). Elliptical annotations on the graphs indicated the most convenient region according to the respective metric (low CoP and high CWR, respectively). As expected, the optimal device changes with the optimality metric. In fact the highest AEP, the highest CWR and the lowest CoP are achieved by three significantly different individuals. In particular, it is evident that the increase in AEP is slower than the required increase in cost, so that the lowest CoP is found in the low cost region, in spite of a lower AEP. Moreover, low-CoP devices have also low CWRs, demonstrating the fact that the main driver is the device cost. Conversely, achieving high CWR and/or high AEP typically requires such an increase in device cost that the overall conversion becomes economically unfavourable.

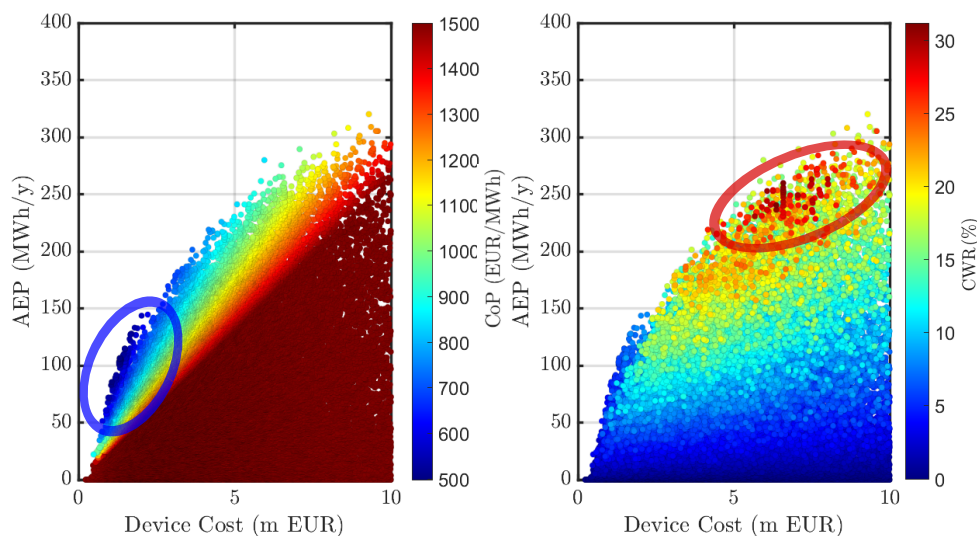


Figure 11. Productivity versus cost of the ensemble of the three optimisations aggregated; with each marker (individual), colour is proportional to the CoP (left) and capture width ratio (CWR) (right). The elliptical annotation highlight the most convenient region according to the evaluation metric (low CoP and high CWR).

It is interesting to analyse the direction that each optimisation tries to follow in order to improve performance index. Figure 12 shows a map of CWR versus COE, with three shaded areas encompassing individuals generated according to the three optimisation objectives. Individuals are also represented by markers of the same colour of the respective shaded area. As expected, the COE-driven area

is attracted towards the bottom CoP-axis and achieves the overall minimum CoP. Similarly the CWR-driven optimisation extends the furthest along the CWR-axis, while obtaining higher CoP. In between, the weighted optimisation reaches good compromises of the two metrics.

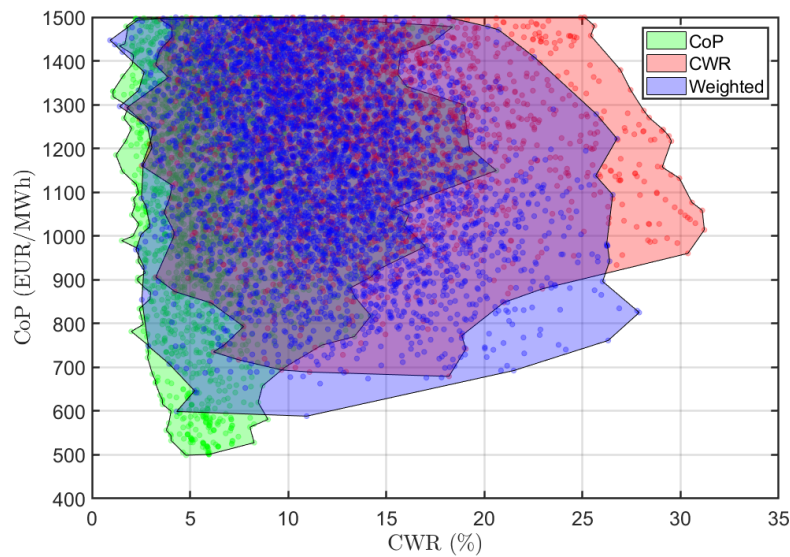


Figure 12. Ensemble of the three optimisations (CoP-driven, CWR-driven and weighted), with shaded areas encompassing each one of the three populations.

Overall, it is important to remark that the CWR-driven optimum has a significantly high CoP, twice the overall minimum CoP. Similarly, also the device with lowest CoP from the CWR-driven optimisation has a high CoP, compared to the entire populations. Conversely, the lowest CoP is obtained by a device with a CWR 6 times smaller than the highest-overall CWR.

From Figure 12 it is possible to extract the Pareto front, shown in Figure 13. Moreover, it is interesting to highlight the evolution of the Pareto front as the algorithm advances through generations. Five different stages of progression are shown, equally spaced from 0% to 100% progression. It is evident that an abrupt improvement is achieved in early stages of the optimisation. Afterwards, although the improvement slows down, the Pareto front is gradually improved, moving downwards and rightwards, namely, to lower CoP and higher CWR.

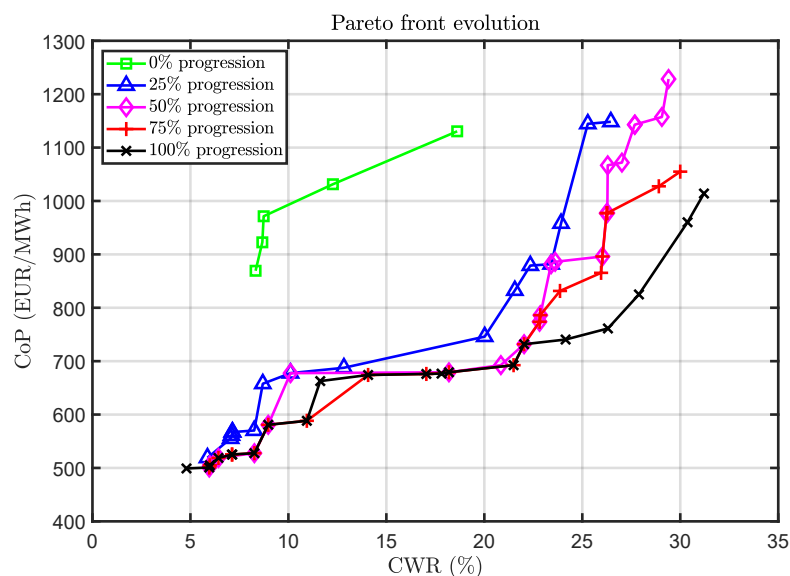


Figure 13. Evolution of the Pareto front, from 0% to 100% progression.

4.1. CoP and CWR Optima

The characteristics of the optimum devices according to different objective functions are hereafter discussed. Figures 14 and 15 show the cross-section and the top-view, respectively, of the optimal devices according to the three optimisations; namely, the CoP-driven optimum, the weight-driven optimum and the CWR-driven optimum. The same axis scale and dimension are used in order to highlight differences in size. Moreover, position, size and number of pendulums are shown.

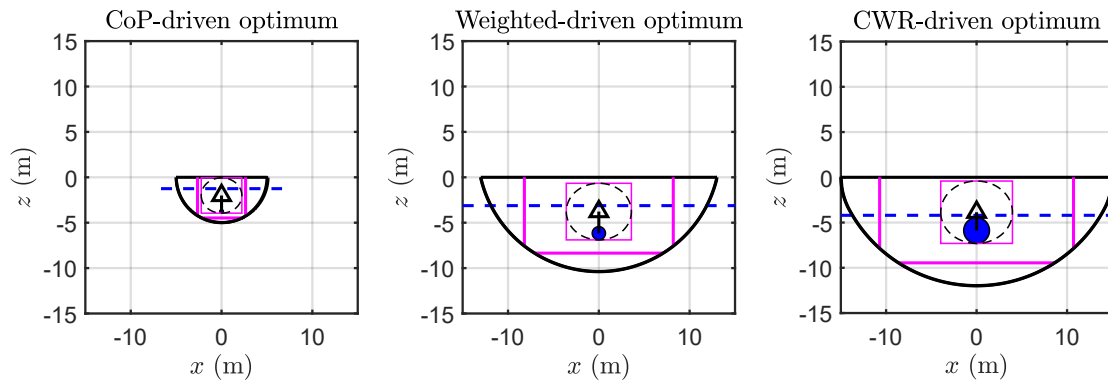


Figure 14. Cross-section of the CoP-driven, the weight-driven and the CWR-driven optima, with common scale and axis dimensions. The pink rectangles represents the ballast compartments and the bulk of the unit. The blue circle is the cross-section of the pendulum mass. The triangular marker represents the fulcrum. The blue dashed line is the still water level.

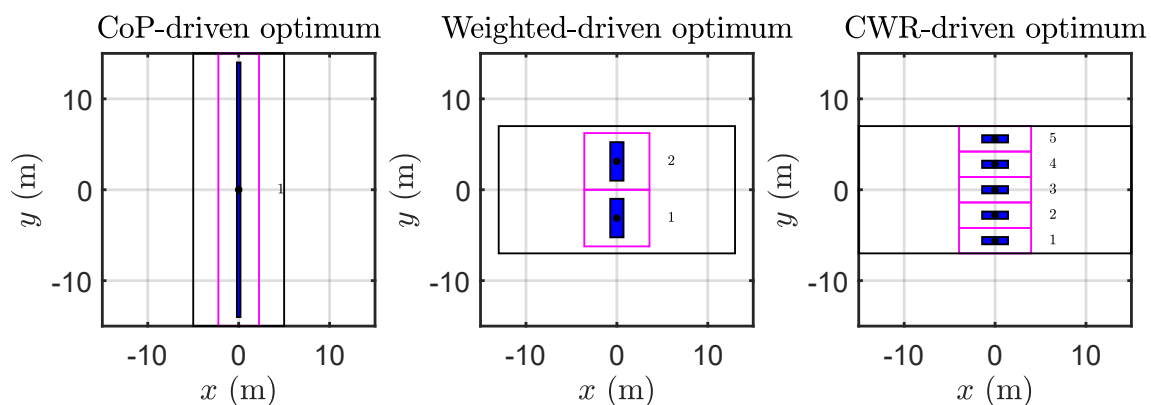


Figure 15. Top view of the CoP-driven, the weight-driven and the CWR-driven optima, with common scale and axis dimensions. The pink rectangles represents the bulk of the unit. The blue rectangle is the pendulum mass.

Clearly, dimensions in the $x - z$ plane increase from left (CoP-driven) to right (CWR-driven), suggesting that a long and high hull is more hydrodynamically efficient for the considered installation site. However, the CoP-optimum is wider than the CWR-optimum, intercepting more wave-crest, hence the high amount of incoming energy. This suggests that increasing the width requires a lower increment in cost than the consequent increase in AEP, hence lowering the resulting CoP. Moreover, the number of pendulums (and PTOs) increases from left to right, hinting that the cost of the PTO is a limiting constraint in the CoP-driven optimisation. Conversely, higher CWR requires more pendulums with larger cross sectional areas and smaller radius/length ratios.

Figure 16 shows the response amplitude operator (RAO) of the CoP-optimum (left) and CWR-optimum (right), for the pitch (RAO_{55} , top) and pendulum oscillation (RAO_{77} , bottom) degrees of freedom. The PTO-free RAO is shown in solid lines and square markers, showing that the natural attitudes of the devices differ according to the pursued objective. In particular, maximising

the CWR leads to a higher natural period (about 7 s) than optimising the CoP (about 5.4 s), so that it can be inferred that converting lower energetic waves (lower period) is more economically convenient. Furthermore, Figure 16 also shows RAOs, including optimal control parameters, shown in Figure 17, which significantly modify the dynamics of the system in order to maximise the performance, while remaining compliant with technical constraints. Since the PTO acts directly on the pendulum (under-actuated system), RAO_{77} is more affected by the control, with significant increases in amplitude and bandwidth. Conversely, the RAO_{55} is damped out, due to the inertial coupling between the hull and the pendulum. Overall, the control increases the energy flux from the hull to the pendulum, and ultimately, the PTO.

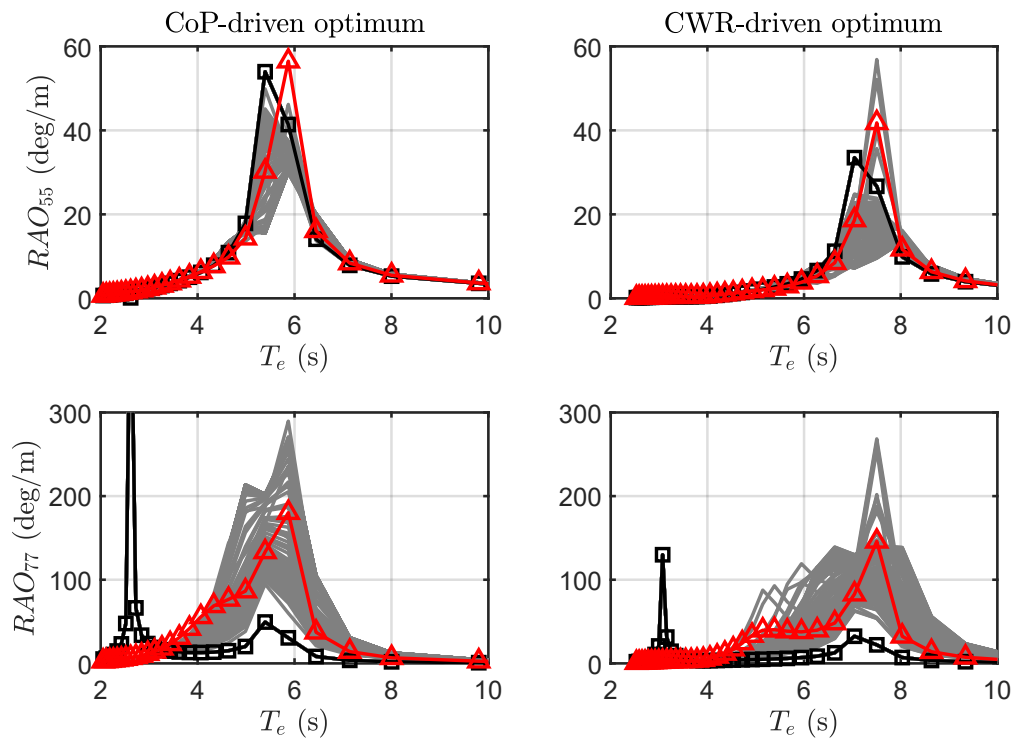


Figure 16. Response amplitude operator of the CoP-optimum (left) and CWR-optimum (right), for the pitch (RAO_{55} , top) and pendulum oscillation (RAO_{77} , bottom) degrees of freedom. The black solid line with square markers is for the PTO-free condition. The set of grey RAO lines is for the various controlled conditions, shown in Figure 17, among which a representative example is the red solid line with triangular markers, referring to c_{PTO} and k_{PTO} weighted over the occurrences matrix.

Overall, Figure 16 highlights the importance of a controlled-informed optimisation. In fact, the algorithm selects a device that is structurally apt to perform well when controlled, as opposed to select a performing uncontrolled device, and then applies a control.

Figure 17, in accordance with Figure 16, shows that the peak of conversion efficiency, i.e., CWR, is around lower wave periods for the CoP-optimum than the CWR-optimum. The control parameters maps show that c_{PTO} is higher for the CWR-driven optimum, since it has to apply a higher damping torque to convert power in higher-energetic sea states. The reactive term of the PTO control, i.e., k_{PTO} , is negative almost across the whole scatter in order to obtain the resonant period of the pendulum T_{res} , shown in the last row of Figure 17. The natural period of the pendulum can be affected by the properties of the pendulum (mass, inertia and length) and k_{pto} . However, the inertial properties of the pendulum also affect the coupling between hull and pendulum, as shown in the off-diagonal terms of (5) and (4), while k_{pto} only affects the diagonal term of the pendulum. Therefore, it appears that the control-informed optimisation algorithm favours lighter pendulums with negative k_{PTO} rather than heavier pendulums and higher k_{PTO} .

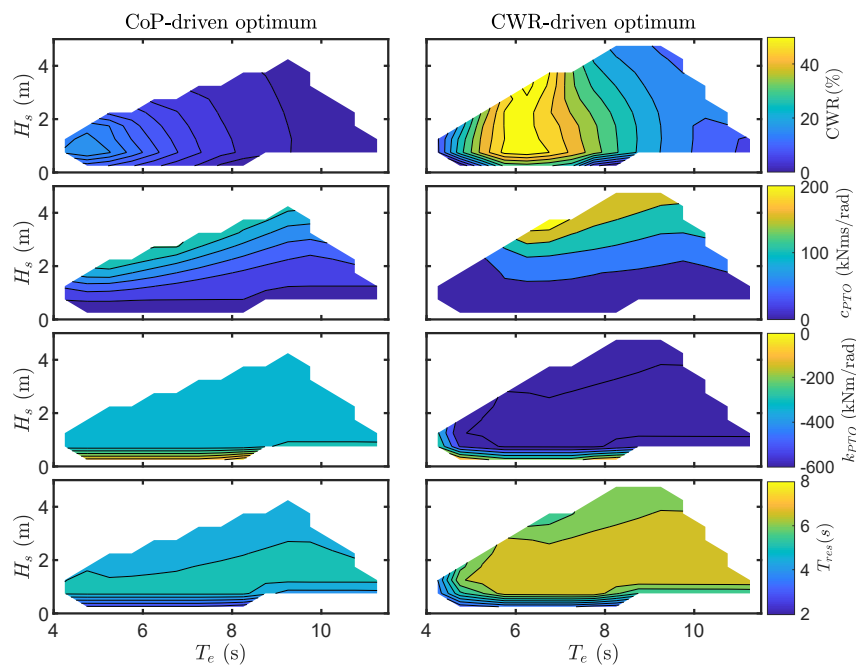


Figure 17. Capture width ratio, reactive control parameters and resonant period of the pendulum for the CoP-driven and CRW-driven optima. The same colour bar is used for each row, in order to favour comparison.

4.2. Techno-Economic Trends and Considerations

It is important to remark that Figures 14 and 15, although representative, are just three examples. Moreover, comments so far have no general or absolute validity, since many interrelated parameters comes into play. In order to investigate significant and more informative trends, Figures 18–21 show relevant results and design parameters for a selection of 28 devices, chosen in order to be representative of the fittest individuals in the whole population, according to the two evaluation metrics considered (CWR and CoP). In practice, the range of CWR from 0% to 30% is equally divided into 14 bins, and the individual with highest CWR of each bin is selected. Likewise, the range of CoP from 500 EUR/MWh to 1000 EUR/MWh is equally divided into 14 bins, and the individual with lowest CoP of each bin is selected. In order to highlight the most convenient individual, according to each metric, bars colour is proportional to CWR and 1/CoP, for the left and right graphs, respectively, so that best devices are represented by blue bars, while worst devices are in red.

The first row of Figure 18 highlights that high CWRs consistently result in high CoPs and vice versa, remarking that conversion efficiency and economic ability can be contrasting objective. It follows that the best devices in the CWR sense (blue bars in the left column) have high CoP. Conversely, the best devices in the CoP sense (blue bars in the right column) are economically performant in spite of their low CWR. In fact, the second and third rows of Figure 18 show that high AEPs come at high device costs and their ratio is more convenient at low AEP.

Figure 19 explores variations in the hull dimensions, which are the main drivers of hydrodynamic performance, and consequent mass, which is proportional to the hull cost. On the one hand, while CWR consistently increases with the hull length, longer hulls generate high CoP. Conversely, the device width is about constant for all CWR and CoP bins, with strong variations just around the second and third bins of the CWR and CoP scales, respectively. Finally, mainly as a consequence of length and width trends, the hull mass increases for increasing CWR and CoP. In particular, low CoP devices require lighter and cheaper hulls.

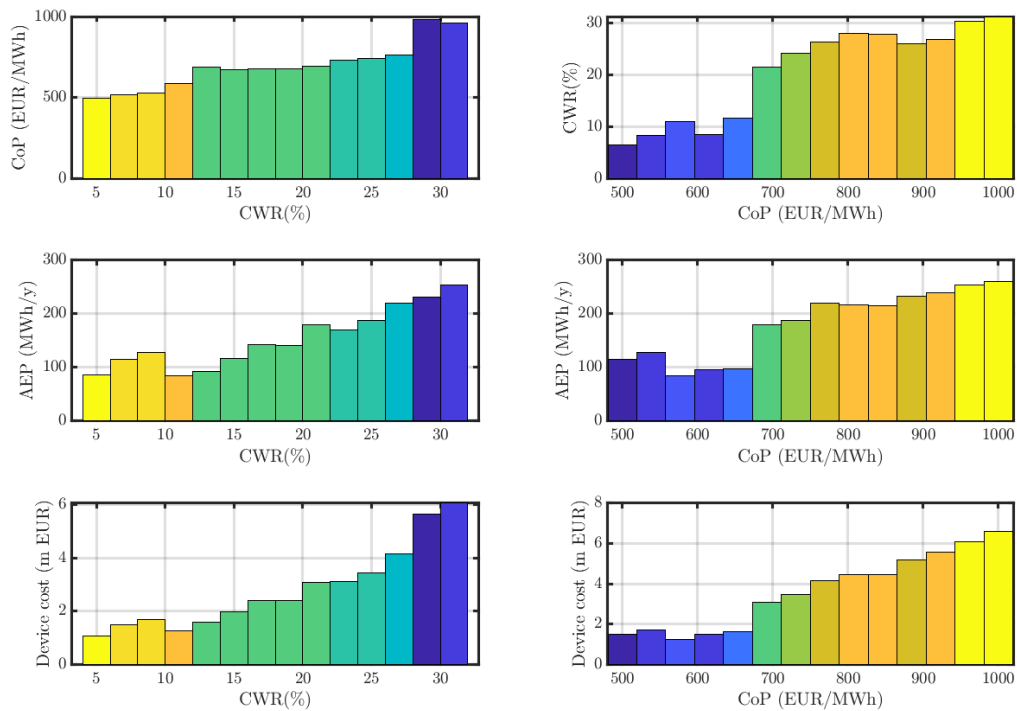


Figure 18. On the left: 14 individuals with the highest CWRs for each CWR-bin, with bars coloured proportionally to CWR. On the right: 14 individuals with the lowest CoPs for each CoP-bin, with bars coloured proportionally to 1/CoP.

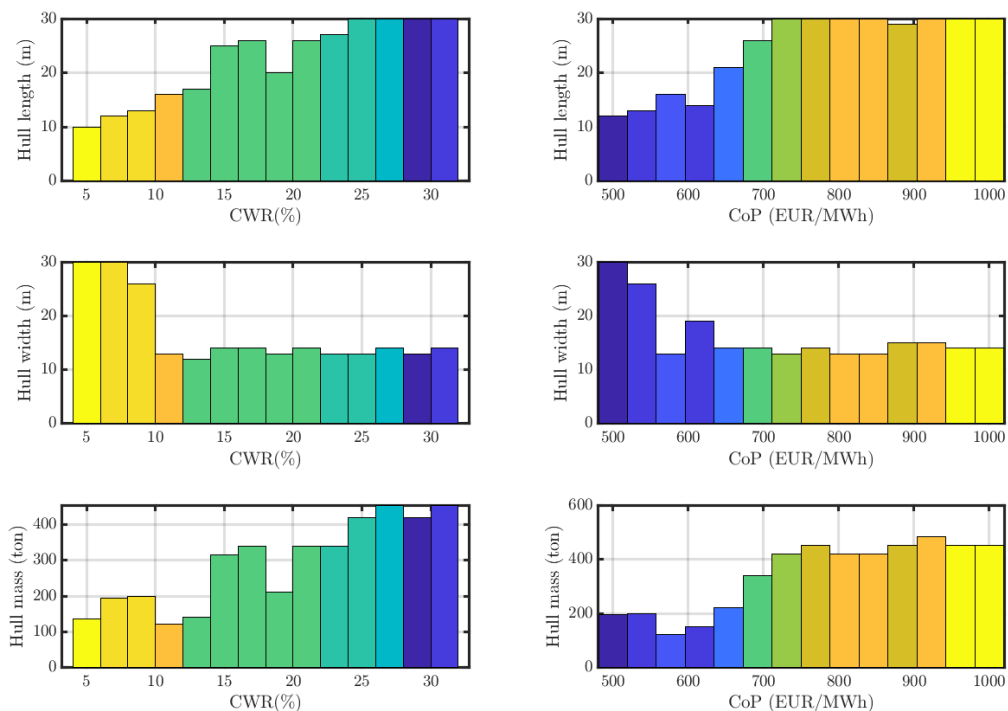


Figure 19. On the left: 14 individuals with highest CWR for each CWR-bin, with bars coloured proportionally to CWR. On the right: 14 individuals with lowest CoP for each CoP-bin, with bars coloured proportionally to 1/CoP.

Figure 20 shows the total pendulum mass, the geometry ratio and the number of pendulums. The cost of the unit is proportional to the total masses of pendulums and their numbers, since there is one PTO attached to each pendulum. Figure 20 shows that more and overall heavier pendulums

increase the CWR but also the CoP, in a similar trend found for the hull dimension and mass, confirming that the incremental investment required to produce more energy is not cost-effective. However, since the pendulums mass and number of pendulums follow the same trend, the single pendulum has about a constant mass in all bins. The geometry ratio σ_p defines how slender the pendulum is, considering the available space. Overall, although no strong correlation is found, it seems that once the masses and number of pendulums are defined, the algorithm leads to cylinders as long and slim as possible (high σ_p).

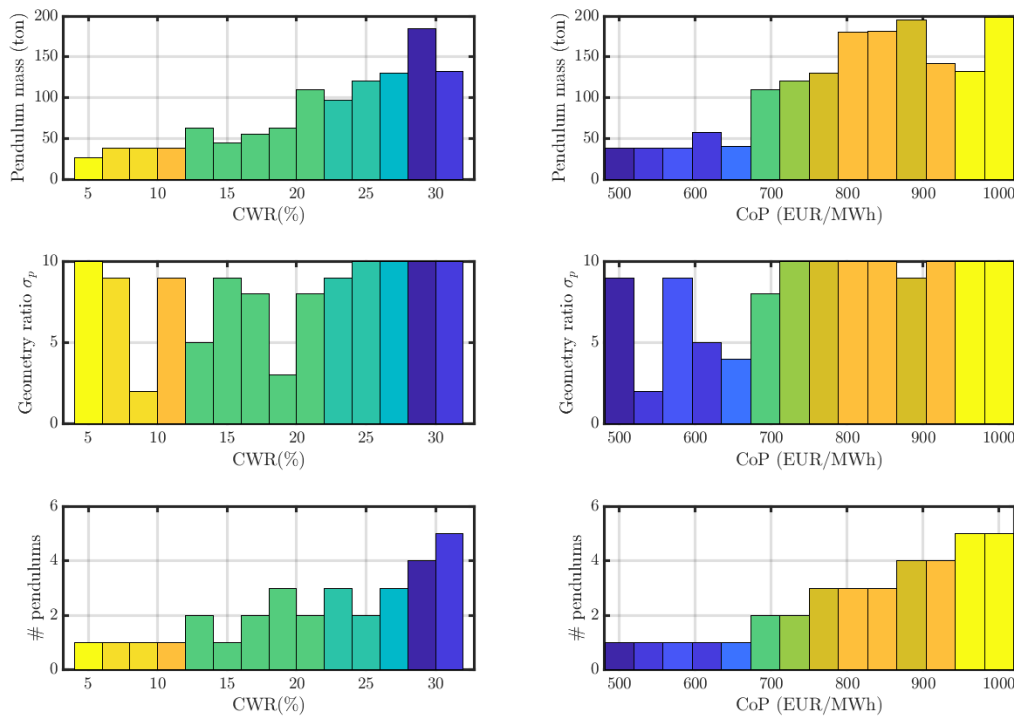


Figure 20. On the left: 14 individuals with the highest CWRs for each CWR-bin, with bars coloured proportionally to CWR. On the right: 14 individuals with the lowest CoPs for each CoP-bin, with bars coloured proportionally to 1/CoP.

Figure 21 shows that CWR and CoP are not particularly sensitive to the single-PTO parameters. In fact, the gearbox ratio is almost always the highest available, while the highest rated torque is often selected, despite the absence of a clear trend, especially in the CWR bins. Similarly, the rated torque is about equally split across both CWR and CoP bins, without any significant pattern. Consequently, the PTOs affect the performance mainly by means of their number, since there is an equal number of PTOs and pendulums: as the optimisation seeks more torque to increase the power conversion, since the largest PTO is already used, the number of pendulum units is increased. Likewise, it seems more cost effective to have fewer pendulums with the largest PTOs than more pendulums with small-medium PTOs.

Finally, Figure 22 shows the total and percentage costs, divided in the hull, pendulum and PTO subcomponents. On the one hand, the absolute cost of each subcomponent tends to increase with both CWR and CoP. On the other hand, the rates of increase seem to be different, since the hull tends to become less relevant in favour of the pendulum/PTO unit. Although the mass (and cost) of the hull increases (from 300 tons to 450 tons), as shown in Figure 19, the number (and cost) of pendulums/PTOs increases at a higher rate (from 1 to 5), as shown in Figure 20. Therefore, Figure 22 shows that the proportional increase of pendulum units has a higher impact than the increase of hull dimension and mass. Alternatively, it can be inferred that the optimisation algorithm reduces the number of

pendulum units in order to reduce the CoP. Conversely, in order to increase the CWR, regardless of subcomponents cost, there must be a higher number of conversion units.

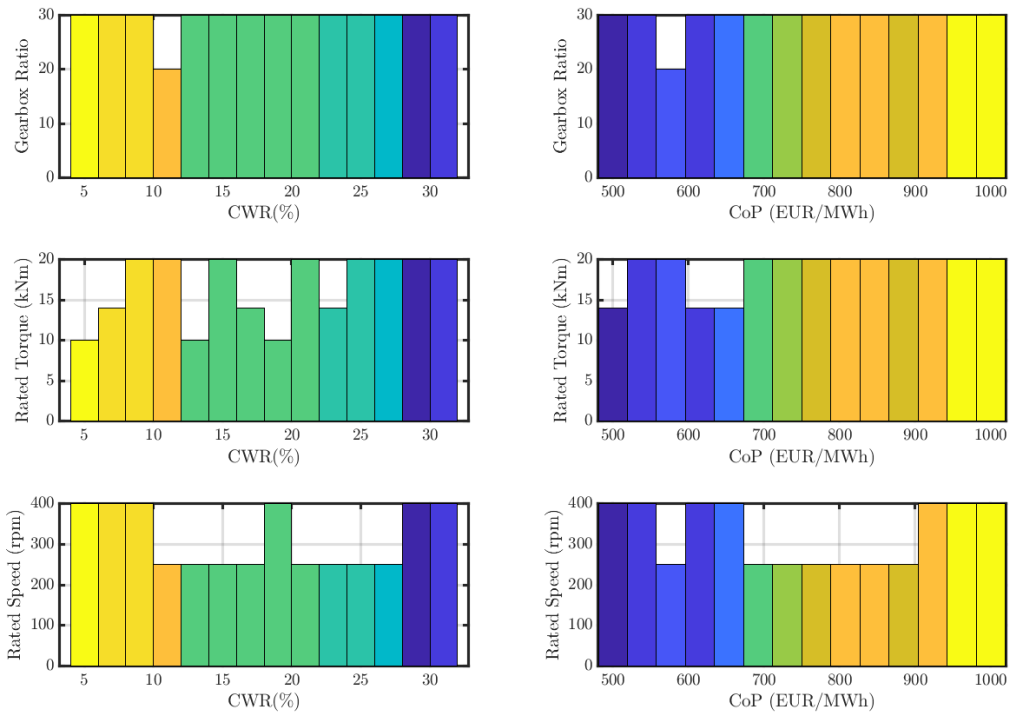


Figure 21. On the left: 14 individuals with the highest CWRs for each CWR-bin, with bars coloured proportionally to CWR. On the right: 14 individuals with lowest the CoPs for each CoP-bin, with bars coloured proportionally to 1/CoP.

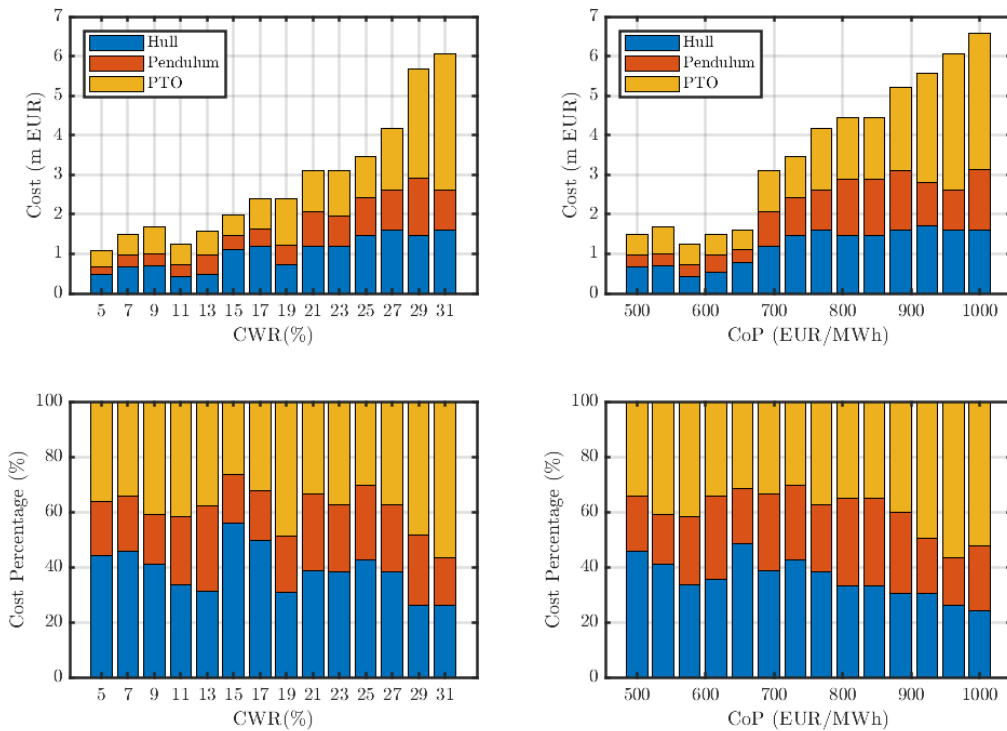


Figure 22. Hull, pendulum and PTO absolute and percentage cost. On the left: 14 individuals with the highest CWRs for each CWR-bin. On the right: 14 individuals with the lowest CoPs for each CoP-bin.

The results discussed so far highlight a limitation of the current concept, which is also an opportunity for substantial improvement. In particular, CWR and CoP are partially competing objectives, due to intrinsic limitations and assumptions. In all configurations, while the largest PTO and gearbox ratio possible are selected, the numbers of pendulum/PTO units are mainly selected in order to either maximise CWR or minimise CoP. Therefore, if the total cost of the PTO system could be decreased while maintaining the same conversion ability, both CWR and CoP would benefit. This can be achieved by connecting each PTO to more than one pendulum. However, since this solution implies requiring an even higher PTO torque, electrical generators become ill-suited. Conversely, hydraulic PTOs work better with high loads at low speed, so the gearbox could also be removed. Moreover, virtually, just one hydraulic PTO could be connected to all pendulums by means of an appropriate hydraulic system. Although the hydraulic PTO system introduces more power losses, the overall cost benefits could lead to a significantly lower CoP.

5. Conclusions

The present paper tackles a comprehensive techno-economic optimisation of a floating wave energy converter via genetic algorithm, considering a wide multi-variate design space, including shape and dimensions of the floater, and subcomponent configuration and characteristics. It is crucial to consider both power conversion ability and total cost of the device, taking physical constraints and control into account for a realistic assessment of the overall performance. Results herein presented are preliminary and not meant to have general validity since they are the consequence of specific techno-economic assumptions and hypotheses on the working principle and configuration. However, there is general validity in stating that the optimisation objective has a great influence on the optimised design, so it should be carefully chosen to be as close as possible to the actual intended target. In this paper it is shown that *efficient* conversion does not necessarily imply *economical* conversion. On the contrary, for the specific case analysed, it resulted that increasing conversion efficiency required an excessive increase in costs, so that the most convenient solution in the economic sense had a relatively low conversion efficiency. Moreover, specific and detailed techno-economic considerations at an early design optimisation stage can lead to substantial conceptual modifications of the system, impossible at a mature development stage, which may be key for the success of such technology.

Author Contributions: Conceptualisation, L.F., S.A.S., G.G., M.B., G.C., G.B. and G.M.; methodology, L.F., S.A.S., G.G., M.B., G.C., G.B. and G.M.; software, L.F., S.A.S., G.G., M.B.; validation, L.F., S.A.S., G.G., M.B.; formal analysis, L.F., S.A.S., G.G., M.B.; investigation, L.F., S.A.S., G.G., M.B., and G.C.; resources, G.G., G.B. and G.M.; data curation, L.F., S.A.S.; writing—original draft preparation, L.F., S.A.S. and G.G.; writing—review and editing, L.F., S.A.S., G.G. and G.C.; visualisation, L.F., S.A.S., G.G. and G.C.; supervision, G.B. and G.M.; project administration, G.B. and G.M.; funding acquisition, G.G., G.B. and G.M. All authors have read and agreed to the published version of the manuscript.

Funding: This research has received funding from the Italian National Agency for New Technologies, Energy and Sustainable Economic Development (ENEA), under the project PTR-PTR_19_21_ENEA_PRG_7. Furthermore, this research was also partially funded by the European Research Executive Agency (REA) under the European Union's Horizon 2020 research and innovation programme under grant agreement No 832140.

Acknowledgments: Computational resources provided by hpc@polito (<http://hpc.polito.it>).

Conflicts of Interest: The authors declare no conflict of interest. The funders had no role in the design of the study; in the collection, analyses, or interpretation of data; in the writing of the manuscript, or in the decision to publish the results.

Appendix A. Genetic Algorithm

Genetic algorithms find their best applications in complex and multi-dimensional optimisation problems, especially those with no analytical formulation of cost and constraint functions. The usual way to handle constraints is via penalty functions, worsening the fitness value in order to avoid unfeasible individuals to proceed in the optimisation. However, in approaches implementing multi-level [48] or dynamic [49] penalty functions, deciding on the penalty parameter is challenging. Moreover, since there

is no direct analytical formulation of the constraints based on the input variables, specific constraint handling based on the knowledge of the mathematical structure (such as the cutting plane method, reduced gradient method or gradient projection method) is not applicable. On the other hand, since genetic algorithms are population based, pair-wise comparison tournament selection is possible [19]. In a tournament, no penalty parameter is required, but only a one-to-one comparison of the severity of the constraint violation. The design optimisation problem presents real variables, which can be handled more efficiently than binary variables, also avoiding the Hamming-Cliff effect [50]. Moreover, in order to improve the convergence rate, variables are defined in a discrete way through integers. The size of each step for each variable is decided by the engineer, based on common sense and previous experience. In this way, the number of possible combinations is reduced, and only significant variations of control parameters are allowed.

Based on previous consideration, the MI-LXPM genetic algorithm has been chosen; it is schematically shown in Figure A1, where:

- **MI:** mixed-integer [51];
- **LX:** Laplace crossover [52];
- **PM:** power mutation [53].

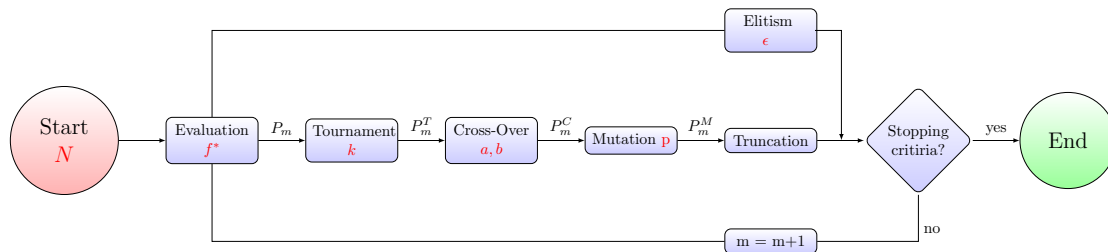


Figure A1. Flowchart of the MI-LXPM genetic algorithm. All phases are described in detail in Appendixes A.1–A.6. Major tuning parameters of the genetic algorithm are shown in red in the flow chart, and summarised in Table 4.

Appendix A.1. Optimisation Problem

The optimisation problem under study can be framed as the minimisation of a generic scalar function $f(x)$ of a vector x , subject to various scalar constraints $g_i(x)$. Note that functions f and g_i present a notional dependence on x , which does not necessary require an explicit mathematical formulation, since they can be evaluated via numerical simulation. Furthermore, each element $x(j)$ of the input vector x is bounded, with $x^L(j)$ being the lower bound and $x^U(j)$ being the upper bound. Finally, note that all elements of x have discrete variations, defined as integer times appropriate steps. Therefore, the optimisation problem can be presented as follows:

$$\begin{aligned}
 & \min_x \quad f(x) \\
 & \text{subject to} \quad g_i(x) \geq 0 \quad \forall i, \\
 & \quad \quad \quad x^L(j) \leq x(j) \leq x^U(j) \quad \forall j.
 \end{aligned} \tag{A1}$$

Constraints are enforced by applying a parameter-free penalty to the objective function when there is a constraint violation. As a condition, constraint functions $g_i(x)$ should also express the severity of the constraint violation, so that ranking between unfeasible position is possible. Therefore, the following fitness index (f^*) is defined:

$$f^*(x) = \begin{cases} f(x) & \text{if } g_i(x) \geq 0 \quad \forall i, \\ f_{\text{death}} + \frac{\Delta_C}{C} & \text{otherwise} \end{cases} \tag{A2}$$

where f_{death} is a death penalty and $\frac{\Delta c}{c}$ represents the distance from of the unfeasible point to the violated constraint, normalised by the constraint itself, as shown in Figure A2. Note that, if f is bounded, f_{death} should be higher than the upper boundary. If f has no upper-boundary, then f_{death} can be iteratively updated with the maximum f until the current generation. Such a formulation, advantageous in handling feasibility and high mortality rates, requires and is made possible by a tournament-type selection of the fittest individuals, as explained in Appendix A.3.

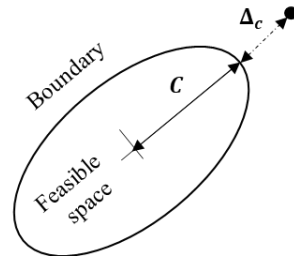


Figure A2. Schematic representation of the constraint violation handling, with reference to (A2).

Appendix A.2. Initial Population and Stopping Criteria

The algorithm starts from an initial population of N individuals, randomly chosen in the design space. The success and computational requirements of the optimisation depend, among other things, on N , which should be large enough to ensure diversification of the genetic code, but not excessively large, which would demand longer simulation time to progress through generations.

In each iteration m of the algorithm, with $m = 1$ at the start, the population P_m goes through a tournament stage, a crossover stage, a mutation stage, and a truncation stage, described in Appendixes A.3–A.6, respectively. In this process, the population is appropriately modified in order to eventually reach a global optimum. However, according to the elitism principle, at each iteration there is a small percentage (ϵ) of the current population which by-passes the mixing-scheme without modifying its genetic information. Such an elite group is formed by the best individuals, whose genetic information should be passed down to the next generation.

The algorithm iterates until one of the two following stopping criteria is met:

- (a) The relative variation of the best fitness index (f_{min}^*) over the previous M_Δ generations is less than a threshold tolerance Δ ;
- (b) The generation count m reaches the allowed limit (M).

Satisfying criterion (a) represents a successful convergence to a minimum. If the population is large enough and with appropriate genetic algorithm parameters (see following sections), such a minimum can be confidently assumed to be also the absolute minimum within given boundaries. On the contrary, if the exit condition is (b), either Δ is overly strict, or the algorithm did not converge, so the tuning parameters of the algorithm should be adjusted.

Appendix A.3. Tournament

The tournament stage implements the survival-of-the-fittest principle by creating an appropriate mating pool P_m^T , where P_m^T stands for the m -population P_m after the tournament phase (T). In each tournament, there are k individuals competing, where k is the tournament size. The winner of each tournament is copied in the mating pool and can continue competing. Every individual takes part to exactly k tournaments so that $(1 - \epsilon)N$ tournaments are played, and in turn, the mating pool is finally populated by $(1 - \epsilon)N$ individuals. It is worth noting that the best-overall individual wins all matches, hence sending k copies of itself into the mating pool and ensuring higher chances to pass their genes over to the next generation. Conversely, the worst-overall individual loses all matches and disappears from the population. In each tournament, the k individuals are compared in pairs until the one that

wins all comparisons is found.. If both individuals are feasible, the one with lowest fitness value wins. If only one is feasible, it survives. If both individuals are unfeasible, the one with lowest constraint violation wins.

Appendix A.4. Laplace Crossover

The crossover phase aims at appropriately mixing genetic information of two parents, randomly taken within the mating pool P_m^T , hence generating a set of off-springs, two from each parents, in order to preserve the total number of individuals. The population of off-springs is called P_m^C , which refers to the m-population P_m after crossover (C). The mixing of information should be a compromise between the need to preserve optimal characteristics of the parents and introducing variability in the genetic code.

Let us consider two arbitrary individuals n_1 and n_2 from the m-population mating pool, namely $(x_{n_1}^T, x_{n_2}^T) \in P_m^T$. Two off-springs are generated, namely $(x_{n_1}^C, x_{n_2}^C) \in P_m^C$, in the following manner:

$$x_n^C(j) = x_n^T(j) + \beta_j \left| x_{n_1}^T(j) - x_{n_2}^T(j) \right|, \quad \forall j \text{ and } n \in [n_1, n_2] \tag{A3}$$

where β_j satisfies the Laplace distribution thanks to the following formulation:

$$\beta_j = \begin{cases} a - b \log(u_j), & \text{if } r_j \leq \frac{1}{2} \\ a + b \log(u_j), & \text{if } r_j > \frac{1}{2} \end{cases} \tag{A4}$$

with u_j and r_j uniform random numbers between 0 and 1, a the location parameter (usually set to 0) and $b > 0$ the scaling parameter. From (A3) and (A4), it is clear that the scaling parameter determines how far the off-springs fall from the parents, hence affecting the convergence rate and success.

Appendix A.5. Power Mutation

Once off-springs are generated, it is necessary to add random variations in the population in order to appropriately investigate the whole design space and avoid the risk of convergence to a local but not global minimum. This is the objective of the mutation phase, generating the P_m^M population, referring to the m-population P_m after mutation (M). A power-distribution mutation scheme is adopted, creating a new individual x_n^M in the proximity of x_n^C as follows:

$$x_n^M(j) = \begin{cases} x_n^C(j) - s_j^p (x_n^C(j) - x^L(j)), & \text{if } t_j < r_j \\ x_n^C(j) + s_j^p (x^U(j) - x_n^C(j)), & \text{if } t_j \geq r_j \end{cases}, \quad \forall j \tag{A5}$$

with

$$t_j = \frac{x_n^C(j) - x^L(j)}{x^U(j) - x_n^C(j)} \tag{A6}$$

and s_j and r_j uniform random numbers between 0 and 1, and p is the index of mutation, determining the strength of the perturbation induced by the power mutation. It follows that, if $p < 1$, s_j^p is statistically closer to 1, amplifying the mutation; conversely, if $p > 1$, s_j^p is statistically closer to 0, attenuating the mutation [51].

Appendix A.6. Truncation

In general, after crossover and mutation, design variables are real values different from the discrete set in the problem definition, shown in (A1). Therefore, for each individual, each element is randomly approximated to either the discretised input variable right below or above, with equal probability. Such an approach ensures to keep the optimisation problem discrete, while adding further randomness in the process.

References

1. Gunn, K.; Stock-Williams, C. Quantifying the global wave power resource. *Renew. Energy* **2012**, *44*, 296–304. [[CrossRef](#)]
2. Weber, J. WEC Technology Readiness and Performance Matrix—Finding the best research technology development trajectory. In Proceedings of the 4th International Conference on Ocean Energy (ICOE), Dublin, Ireland, 17–19 October 2012; pp. 1–10.
3. Weber, J.; Roberts, J. Cost, time and risk assessment of different wave energy converter technology development trajectories. In Proceedings of the Twelfth European Wave and Tidal Energy Conference, Cork, Ireland, 27 August–1 September 2017.
4. Penalba, M.; Ringwood, J.V. A high-fidelity wave-to-wire model for wave energy converters. *Renew. Energy* **2019**, *134*, 367–378. [[CrossRef](#)]
5. Genuardi, L.; Bracco, G.; Sirigu, S.A.; Bonfanti, M.; Paduano, B.; Dafnakis, P.; Mattiazzo, G. An application of model predictive control logic to inertial sea wave energy converter. In *Mechanisms and Machine Science*; Springer Nature: Heidelberg, Germany, 2019; Volume 73, pp. 3561–3571. [[CrossRef](#)]
6. Bracco, G.; Casassa, M.; Giorcelli, E.; Giorgi, G.; Martini, M.; Mattiazzo, G.; Passione, B.; Raffero, M.; Vissio, G. Application of sub-optimal control techniques to a gyroscopic Wave Energy Converter. *Renew. Energ. Offshore* **2014**, *1*, 265–269.
7. Sirigu, A.S.; Gallizio, F.; Giorgi, G.; Bonfanti, M.; Bracco, G.; Mattiazzo, G. Numerical and Experimental Identification of the Aerodynamic Power Losses of the ISWEC. *J. Mar. Sci. Eng.* **2020**, *8*, 49. [[CrossRef](#)]
8. de Andres, A.; Maillet, J.; Todalshaug, J.H.; Möller, P.; Bould, D.; Jeffrey, H. Techno-economic related metrics for a wave energy converters feasibility assessment. *Sustainability* **2016**, *8*, 1109. [[CrossRef](#)]
9. Farrell, N.; Donoghue, C.; Morrissey, K. Quantifying the uncertainty of wave energy conversion device cost for policy appraisal: An Irish case study. *Energy Policy* **2015**, *78*, 62–77. [[CrossRef](#)]
10. Giorgi, G.; Ringwood, J.V. Analytical formulation of nonlinear Froude-Krylov forces for surging-heaving-pitching point absorbers. In Proceedings of the ASME 2018 37th International Conference on Ocean, Offshore and Arctic Engineering, Madrid, Spain, 17–22 June 2018.
11. Giorgi, G.; Ringwood, J.V. Articulating parametric nonlinearities in computationally efficient hydrodynamic models. In Proceedings of the 11th IFAC Conference on Control Applications in Marine Systems, Robotics, and Vehicles, Opatija, Croatia, 10–12 September 2018.
12. Ringwood, J.V.; Merigaud, A.; Faedo, N.; Fusco, F. Wave Energy Control Systems: Robustness Issues. In Proceedings of the IFAC Conference on Control Applications in Marine Systems, Robotics, and Vehicles, Opatija, Croatia, 10–12 September 2018.
13. Ringwood, J.V.; Merigaud, A.; Faedo, N.; Fusco, F. An Analytical and Numerical Sensitivity and Robustness Analysis of Wave Energy Control Systems. *IEEE Trans. Control Syst. Technol.* **2019**, *28*, 1337–1348. [[CrossRef](#)]
14. Giorgi, G.; Ringwood, J.V. Parametric motion detection for an oscillating water column spar buoy. In Proceedings of the 3rd International Conference on Renewable Energies Offshore RENEW, Lisbon, Portugal, 8–10 October 2018.
15. Gilloteaux, J.C.; Ringwood, J.V. Control-informed geometric optimisation of wave energy converters. *IFAC Proc. Vol. (IFAC-PapersOnline)* **2010**, *43*, 366–371. [[CrossRef](#)]
16. Garcia-Rosa, P.; Bacelli, G.; Ringwood, J. Control-Informed Geometric Optimization of Wave Energy Converters: The Impact of Device Motion and Force Constraints. *Energies* **2015**, *8*, 13672–13687. [[CrossRef](#)]
17. Giorgi, G.; Ringwood, J.V. Articulating parametric resonance for an OWC spar buoy in regular and irregular waves. *J. Ocean Eng. Mar. Energy* **2018**, *4*, 311–322. [[CrossRef](#)]
18. Novo, R.; Bracco, G.; Sirigu, S.; Mattiazzo, G.; Merigaud, A.; Ringwood, J. Non-linear simulation of a wave energy converter with multiple degrees of freedom using a harmonic balance method. In Proceedings of the International Conference on Offshore Mechanics and Arctic Engineering (OMAE), Madrid, Spain, 17–22 June 2018; Volume 10. [[CrossRef](#)]
19. Deb, K. An efficient constraint handling method for genetic algorithms. *Comput. Methods Appl. Mech. Eng.* **2000**, *186*, 311–338. [[CrossRef](#)]
20. Götteman, M.; Giassi, M.; Engström, J.; Isberg, J. Advances and Challenges in Wave Energy Park Optimization—A Review. *Front. Energy Res.* **2020**, *8*, 26. [[CrossRef](#)]
21. Birk, L. Application of constrained multi-objective optimization to the design of offshore structure hulls. *J. Offshore Mech. Arct. Eng.* **2009**, *131*, 011301. [[CrossRef](#)]

22. Sharp, C.; DuPont, B. Wave energy converter array optimization: A genetic algorithm approach and minimum separation distance study. *Ocean Eng.* **2018**, *163*, 148–156. [[CrossRef](#)]
23. Giassi, M.; Götteman, M. Layout design of wave energy parks by a genetic algorithm. *Ocean Eng.* **2018**, *154*, 252–261. [[CrossRef](#)]
24. Shadman, M.; Estefen, S.F.; Rodriguez, C.A.; Nogueira, I.C. A geometrical optimization method applied to a heaving point absorber wave energy converter. *Renew. Energy* **2018**, *115*, 533–546. [[CrossRef](#)]
25. Kurniawan, A.; Moan, T. Optimal geometries for wave absorbers oscillating about a fixed axis. *IEEE J. Ocean. Eng.* **2013**, *38*, 117–130. [[CrossRef](#)]
26. McCabe, A.P. Constrained optimization of the shape of a wave energy collector by genetic algorithm. *Renew. Energy* **2013**, *51*, 274–284. [[CrossRef](#)]
27. Cordonnier, J.; Gorintin, F.; De Cagny, A.; Clément, A.H.; Babarit, A. SEAREV: Case study of the development of a wave energy converter. *Renew. Energy* **2015**, *80*, 40–52. [[CrossRef](#)]
28. Pozzi, N.; Bonetto, A.; Bonfanti, M.; Bracco, G.; Dafnakis, P.; Giorcelli, E.; Passione, B.; Sirigu, S.; Mattiazzo, G. PeWEC: Preliminary design of a full-scale plant for the mediterranean sea. In Proceedings of the NAV International Conference on Ship and Shipping Research, Trieste, Italy, 20–22 June 2018; pp. 504–514. [[CrossRef](#)]
29. Ruellan, M.; Benahmed, H.; Multon, B.; Josset, C.; Babarit, A.; Clement, A. Design methodology for a SEAREV wave energy converter. *IEEE Trans. Energy Convers.* **2010**, *25*, 760–767. [[CrossRef](#)]
30. Sirigu, S.A.; Bonfanti, M.; Begovic, E.; Bertorello, C.; Dafnakis, P.; Bracco, G.; Mattiazzo, G. Experimental Investigation of Mooring System on a Wave Energy Converter in Operating and Extreme Wave Conditions. *J. Mar. Sci. Eng.* **2020**, *8*, 180. [[CrossRef](#)]
31. Pozzi, N.; Bracco, G.; Passione, B.; Sirigu Sergej, A.; Vissio, G.; Mattiazzo, G.; Sannino, G. Wave Tank Testing of a Pendulum Wave Energy Converter 1:12 Scale Model. *Int. J. Appl. Mech.* **2017**, *9*, 1750024. [[CrossRef](#)]
32. Sirigu, S.A.; Bonfanti, M.; Passione, B.; Begovic, E.; Bertorello, C.; Dafnakis, P.; Bracco, G.; Giorcelli, E.; Mattiazzo, G. Experimental investigation of the hydrodynamic performance of the ISWEC 1:20 scaled device. In Proceedings of the NAV International Conference on Ship and Shipping Research, Trieste, Italy, 20–22 June 2018; pp. 551–560. [[CrossRef](#)]
33. Pozzi, N. Numerical Modeling and Experimental Testing of a Pendulum Wave Energy Converter (PeWEC). Ph.D. Thesis, Polytechnic of Turin, Torino, Italy, 2018. [[CrossRef](#)]
34. Sirigu, S.; Bonfanti, M.; Dafnakis, P.; Bracco, G.; Mattiazzo, G.; Brizzolara, S. Pitch Resonance Tuning Tanks: A novel technology for more efficient wave energy harvesting. In Proceedings of the OCEANS 2018 MTS/IEEE Charleston (OCEAN 2018), Charleston, SC, USA, 22–25 October 2019. [[CrossRef](#)]
35. Bonfanti, M.; Bracco, G.; Dafnakis, P.; Giorcelli, E.; Passione, B.; Pozzi, N.; Sirigu, S.; Mattiazzo, G. Application of a passive control technique to the ISWEC: Experimental tests on a 1:8 test rig. In Proceedings of the NAV International Conference on Ship and Shipping Research, Trieste, Italy, 20–22 June 2018; pp. 60–70. [[CrossRef](#)]
36. Sirigu, S.A.; Bracco, G.; Bonfanti, M.; Dafnakis, P.; Mattiazzo, G. On-board sea state estimation method validation based on measured floater motion. *IFAC-PapersOnLine* **2018**, *51*, 68–73. [[CrossRef](#)]
37. Giorgi, G.; Gomes, R.P.F.; Bracco, G.; Mattiazzo, G. The effect of mooring line parameters in inducing parametric resonance on the Spar-buoy oscillating water column wave energy converter. *J. Mar. Sci. Eng.* **2020**, *8*, 29. [[CrossRef](#)]
38. Babarit, A.; Delhommeau, G. Theoretical and numerical aspects of the open source BEM solver NEMOH. In Proceedings of the 11th European Wave and Tidal Energy Conference, Nantes, France, 6–11 September 2015; pp. 1–12.
39. Pozzi, N.; Bracco, G.; Passione, B.; Sirigu, S.A.; Mattiazzo, G. PeWEC: Experimental validation of wave to PTO numerical model. *Ocean Eng.* **2018**, *167*, 114–129. [[CrossRef](#)]
40. Fontana, M.; Casalone, P.; Sirigu, S.A.; Giorgi, G. Viscous Damping Identification for a Wave Energy Converter Using CFD-URANS Simulations. *J. Mar. Sci. Eng.* **2020**, *8*, 355. [[CrossRef](#)]
41. Penalba, M.; Giorgi, G.; Ringwood, J.V. Mathematical modelling of wave energy converters: A review of nonlinear approaches. *Renew. Sustain. Energy Rev.* **2017**, *78*, 1188–1207. [[CrossRef](#)]
42. Giorgi, G.; Gomes, R.P.F.; Bracco, G.; Mattiazzo, G. Numerical investigation of parametric resonance due to hydrodynamic coupling in a realistic wave energy converter. *Nonlinear Dyn.* **2020**. [[CrossRef](#)]
43. Lagarias, J.C.; Reeds, J.A.; Wright, M.H.; Wright, P.E. Convergence properties of the nelder–mead simplex method in low dimensions. *SIAM J. Optim.* **1998**, *9*, 112–147. [[CrossRef](#)]

44. Garcia-Teruel, A.; Forehand, D.I.; Jeffrey, H. Wave Energy Converter hull design for manufacturability and reduced LCOE. In Proceedings of the 7th International Conference on Ocean Energy (ICOE), Cherbourg, Normandy, France, 12–13 June 2018; pp. 1–9.
45. Emmerich, M.T.; Deutz, A.H. A tutorial on multiobjective optimization: Fundamentals and evolutionary methods. *Nat. Comput.* **2018**, *17*, 585–609. [[CrossRef](#)]
46. Astariz, S.; Iglesias, G. Enhancing Wave Energy Competitiveness through Co-Located Wind and Wave Energy Farms. A Review on the Shadow Effect. *Energies* **2015**, *8*, 7344–7366. [[CrossRef](#)]
47. Miettinen, K. *Nonlinear Multiobjective Optimization*, 1st ed.; Springer: Boston, MA, USA, 1998; p. 298. [[CrossRef](#)]
48. Homaifar, A.; Qi, C.X.; Lai, S.H. Constrained Optimization Via Genetic Algorithms. *Simulation* **1994**, *62*, 242–253. [[CrossRef](#)]
49. Joines, J.A.; Houck, C.R. On the use of non-stationary penalty functions to solve nonlinear constrained optimization problems with GA's. In Proceedings of the First IEEE Conference on Evolutionary Computation (IEEE World Congress on Computational Intelligence), Orlando, FL, USA, 27–29 June 1994; pp. 579–584. [[CrossRef](#)]
50. Cheung, B.K.; Langevin, A.; Delmaire, H. Coupling Genetic Algorithm with a grid search method to solve Mixed Integer Nonlinear Programming problems. *Comput. Math. Appl.* **1997**, *34*, 13–23. [[CrossRef](#)]
51. Deep, K.; Singh, K.P.; Kansal, M.L.; Mohan, C. A real coded genetic algorithm for solving integer and mixed integer optimization problems. *Appl. Math. Comput.* **2009**, *212*, 505–518. [[CrossRef](#)]
52. Deep, K.; Thakur, M. A new crossover operator for real coded genetic algorithms. *Appl. Math. Comput.* **2007**, *188*, 895–911. [[CrossRef](#)]
53. Deep, K.; Thakur, M. A new mutation operator for real coded genetic algorithms. *Appl. Math. Comput.* **2007**, *193*, 211–230. [[CrossRef](#)]



© 2020 by the authors. Licensee MDPI, Basel, Switzerland. This article is an open access article distributed under the terms and conditions of the Creative Commons Attribution (CC BY) license (<http://creativecommons.org/licenses/by/4.0/>).